Title:

Hippocampal single-cell RNA Atlas of chronic methamphetamine abuse-induced cognitive decline in mice.

Authors and Affiliations

H Qiu, X Yue, YB Huang, ZL Meng, JH Wang* and DF Qiao*

H Qiu, Ph.D., School of Forensic Medicine, Southern Medical University.

X Yue, Ph.D., School of Forensic Medicine, Southern Medical University.

YB Huang, M.D., School of Forensic Medicine, Southern Medical University.

ZL Meng, M.D.,School of Forensic Medicine, Southern Medical University.

JH Wang*, Ph.D., Cancer Research Institute, School of Basic Medical Sciences, Southern Medical University, Guangzhou 510515, People' s Republic of China. E-mail address: wjh1987@smu.edu.cn.

DF Qiao*, Ph.D., School of Forensic Medicine,Southern Medical University, Guangzhou Key Laboratory of Forensic Multi-Omics for Precision Identification, Guangzhou 510515, Guangdong province, People' s Republic of China. E-mail address: qiaodf@smu.edu.cn.

*DF Qiao and JH Wang are Corresponding Authors.

Abstract

Background: Chronic methamphetamine abuse leads to cognitive decline, posing a significant threat to human health and contributing to loss of productivity. However, the intricate and multifaceted mechanisms underlying methamphetamine-induced neurotoxicity have impeded the development of effective therapeutic interventions.

Methods: To establish a mouse model of cognitive decline induced by chronic methamphetamine exposure, we employed a large sample size and conducted two behavioral tests (Y-maze and novel object recognition test) at 2 and 4 weeks post-exposure. Subsequently, single-cell RNA sequencing was utilized to delineate the mRNA expression profiles of individual cells within the hippocampus. Comprehensive bioinformatics analyses, including cell clustering and identification, differential gene expression analysis, cellular communication analysis, pseudotemporal trajectory analysis, and transcription factor regulation analysis, were performed to elucidate the cellular-level changes in mRNA profiles caused by chronic methamphetamine exposure.

Results: Our findings demonstrated impairments in working memory, spatial cognition, learning, and cognitive memory. After 4 weeks of behavioral testing, we identified diverse cell types in the hippocampi of METH- and saline-treated mice through scRNA-seq, including glial cells, stromal cells, vascular cells, and immune cells. We observed that methamphetamine exerts cell-specific effects on gene expression changes associated with neuroinflammation, blood-brain barrier disruption, neuronal support dysfunction, and immune dysregulation. Furthermore, cross-talk analysis revealed extensive alterations in cellular communication patterns and signal changes within the hippocampal microenvironment induced by methamphetamine exposure. Pseudotime analysis predicted hippocampal neurogenesis disorders and identified key regulatory genes implicated in chronic methamphetamine abuse. Transcription factor analysis uncovered regulators and pathways linked to astrocyte-mediated neuroinflammation, endothelial junction integrity, microglial

synaptic remodeling, and oligodendrocyte-supported neuronal cell bodies and axons. Additionally, it highlighted the role of neural precursor cells in various forms of neurodegeneration.

Conclusions: This study establishes a robust mouse model of cognitive impairment induced by chronic methamphetamine exposure. It provides valuable biological insights, characterizes the single-cell atlas of the hippocampus, and offers novel directions for investigating neurological damage associated with chronic methamphetamine-induced cognitive decline.

Keywords

Chronic methamphetamine abuse; Cognitive decline; Hippocampus; Single-cell RNA sequencing; Atlas

Introduction

Methamphetamine (METH), a widely abused psychostimulant globally, particularly in southeast and east Asia, currently holds the position of being the world's foremost illicitly manufactured synthetic drug. Its detrimental impact on human health, social stability, and economic development is immense(1). METH induces intense euphoria and addiction, while causing significant harm to various tissues and organs, especially the central nervous system. With advancements in productivity and medical standards, research focusing on neuropsychiatric issues associated with chronic METH abuse has become a prominent topic concerning drug users' treatment, recovery, and quality of life. Chronic and regular usage of METH has been proven to result in an array of brain structural abnormalities such as cortical and hippocampal atrophy, nucleus accumbens hypertrophy, as well as decreased gray matter(2-4), leading to neuropsychiatric disorders including neurodegeneration, cognitive deficits, agitation, paranoia, depression, delusions, and schizophrenia. However, due to the

wide range of affected targets and complex mechanisms underlying METH's effects, the evolution and interplay of these effects during chronic processes make it challenging to analyze the etiology of these neuropsychiatric diseases.

Extensive clinical and experimental evidences suggest that chronic METH abuse leads to cognitive deficits(5-7), which share similarities with neurodegenerative disorders such as impaired inhibitory control, learning and memory decline, attention decrease, increased pathological protein levels, neurotoxicity, neuroinflammation, and blood-brain barrier (BBB) injury. The hippocampus plays a crucial role in regulating cognitive function as part of the limbic system. Previous studies have demonstrated that METH exerts complex negative effects on the hippocampus beyond its direct impact on dopaminergic and glutamatergic systems(8). It also indirectly affects various cell types within the hippocampus and alters the microenvironment. However, due to the intricate composition of the hippocampus and diverse mechanisms underlying METH's effects, certain impacts on vulnerable cell types and critical signaling pathways may be concealed during chronic exposure, making it challenging to unravel these mechanisms. Currently, there is limited understanding of the specific mechanisms responsible for chronic METH-induced neurotoxicity in the hippocampus leading to cognitive deficits; furthermore, theories explaining this wide range of effects are scarce.

In this study, we employed single-cell RNA sequencing (scRNA-seq) to construct a comprehensive hippocampal atlas of chronic METH abuse-induced cognitive decline in mice. To elucidate the underlying mechanisms by which chronic METH abuse affects the hippocampus and leads to cognitive deficits, we conducted animal behavior tests, performed scRNA-seq analysis with clustering and differential gene expression analyses, investigated cellular cross-talk, examined single-cell trajectories, and analyzed transcription factors. This study provides in vivo evidence of heterogeneous changes in hippocampal cells under chronic METH abuse and contributes to a more robust understanding of the mechanistic basis for cognitive deficits while also bridging previous theories on METH neurotoxicity.

Materials and methods

Animal and Treatments

All mice used were male and on C57BL/6 background. Healthy 7-week-old mice were purchased from the Laboratory Animal Center of Southern Medical University (Guangzhou, China). Mice were quarantined for 2 weeks and then housed in the Central Exhaust Ventilation Cage System (Houhuang experimental equipment technology, Suzhou, China) with 12 hours (h) light/12 h dark cycle in a temperature- (20–22 ℃) and humidity- (45–55%) controlled vivarium and had ad libitum access to water and food. All protocols approved by the Institutional Animal Care and Use Committee in Southern Medical University (Ethical number: L2022125), and consistent with NIH Guidelines for the Care and Use of Laboratory Animals (8th Edition, U.S. National Research Council, 2011). After 1 week for adapting, mice were 10 weeks of age at the start of the experiment. They were randomly divided into two groups, and then treated by saline or METH (National Institutes for the Control of Pharmaceutical and Biological Products, Beijing, China). Mice of METH group were intraperitoneally administered METH dissolved in saline at a incremental dose from 1 up to 10 mg/kg, and the daily dose was evenly divided into two doses at 12-hour intervals, while those of saline control underwent the same way of injection with saline simultaneously. The treatments lasted for 28 days. However the last administration of 12 h before animal behavior tests or sample-collecting would be skipped. For scRNA-seq, we used 20 mice (10 from saline group, 10 from METH group, and each random 2 mice from same cage were composed of 1 sample).

Behavioral Experiments

Behavioral testing of mice used for scRNA-seq experiments followed an established protocol. To minimize any stimulation, mice would be handled for 5 days to be habituated to environment and tester (30 min to environment, 5 min to tester)

before behavioral experiments. Less irritating behavioral experiments were used to evaluate in order to minimize impacts on scRNA-seq.

Y-Maze

Y maze test was used to evaluate spontaneous alternation behavior in mice. The Y-maze was made of three arms set at angles of 120°. Its walls are covered with frosted adhesive paper. Mice were placed in the end of fixed arm of Y-maze, then they were allowed to freely explore whole Y-maze for 8-min session while camera system recorded the behavior of mice. The total number of entries of each arm (recognizing that all four legs of mouse entered the arm as the standard for entries), the number of alternations (an alternation is defined as successive entries into the three arms on overlapping triplet sets.), and the ratio of them were regarded as statistical indicators to assess spatial working memory.

Novel Object Recognition Test

Novel object recognition test (NOR) was applied to assess mice recognition memory. The testing room was lit with four LED lights which provide the light intensity of approximately 20 lx in each test box (50 × 50 × 40 cm). Mice were put into test room to habituate for 24h before beginning of test, and would be given 10 min to explore the object-free box and were then returned to their home cage. In training stage, two objects of same appearance were placed at a symmetrical position in test box where mice would explore freely for 10min to be fully acquainted with objects. After training, mice were sent back to their home cage to rest for 30 min. Then in testing stage, they were placed back into original test box with a familiar old object and a novel one at the same place and also allowed to explore freely for 10 min. The familiar object and novel object and their placement were counterbalanced within each group. Camera system was placed above the test box and recorded behaviors of mice in test box for statistics.

153 The following behaviors were scored as exploration: biting, sniffing, licking,
154 touching the object with the nose or with the front legs, or proximity (≤1 cm) between
155 the nose and the object. If the mouse put its hind legs on objects, or stood on top of
156 the object or completely immobile, exploration was not scored. The preference index
157 for the novel object was calculated as (time spent exploring the new object / the total
158 time spent exploring both objects), and the discrimination index was calculated as
159 (time spent exploring the new object − time spent exploring the familiar old object) /
160 (total time spent exploring both objects). Behavior was scored on video by two
161 observers blinded to the mice's treatment.

162 **Brain Samples Collecting**

163 For scRNA-seq, we used hippocampus tissues of 20 mice (10 from saline group,
164 10 from METH group, and each random 2 mice from same cage were regarded as 1
165 sample). Hippocampus collecting was carried out under the guidance of JOVE(8).
166 After the mice were subjected to 3 min of pre-cooling with PBS for cardiovascular
167 perfusion, whole hippocampus was dissected integrally on icein the shortest time
168 (within 5 min) and preserved in tissue preservation solution (SeekGene, China) at 4℃
169 for following tissue dissociation.

170 **Cell Preparation for Sing Cell RNA Sequencing**

171 After harvested, tissues were washed in ice-cold RPMI1640 and dissociated
172 using Tissue Dissociation Reagent A (Seekone K01301-30, China) from SeekGene
173 as instructions. DNase Ⅰ (Sigma 9003-98-9, USA) treatment was optional according
174 to the viscosity of the homogenate. Cell count and viability was estimated using
175 fluorescence Cell Analyzer (Countstar® Rigel S2) with AO/PI reagent after removal
176 erythrocytes (Solarbio R1010, China) and then debris and dead cells removal was
177 decided to be performed or not (Miltenyi Biotec 130-109-398/130-090-101, USA).
178 Finally fresh cells were washed twice in the RPMI1640 and then resuspended at
179 1×10^6 cells/mL in 1×PBS and 0.04% bovine serum albumin.

Single Cell RNA Sequencing Library Construction and Sequencing

Single-cell RNA-Seq libraries were prepared using Chromium Next GEM Single Cell 3' Reagent Kits v3.1 (10x Genomics Catalog No.1000268, USA). Briefly, appropriate number of cells were mixed with reverse transcription reagent and then loaded to the sample well in Chromium Next GEM Chip G. Subsequently Gel Beads and Partitioning Oil were dispensed into corresponding wells separately in chip. After emulsion droplet generation reverse transcription were performed at 53℃for 45 min and inactivated at 85℃ for 5 min. Next, cDNA was purified from broken droplet and amplified in PCR reaction. The amplified cDNA product was then cleaned, fragmented, end repaired, A-tailed and ligated to sequencing adaptor. Finally, the indexed PCR was performed to amplify the DNA representing 3' polyA part of expressing genes which also contained Cell Bar code and Unique Molecular Index. The indexed sequencing libraries were cleanup with SPRI beads, quantified by quantitative PCR (KAPA Biosystems KK4824) and then sequenced on illumina NovaSeq 6000 with PE150 read length.

Processing the Single Cell RNA Sequencing Data and Date Quality Control

The raw sequencing data was processed by Fastp firstly (Chen, Zhou et al. 2018) to trim primer sequence and low quality bases. And then we employed the Cell Ranger software v7.0 (10X Genomics) obtained from https://www.10xgenomics.com/support/software/cell-ranger/downloads to precess sequence data and aligned to mouse mm10 genome in order to obtain gene expression matrix. Subsequently, the gene expression matrices of each sample were obtained and further analyzed using Seurat v.4.4.0. Then we determined effective cells using the following criteria: (a) total UMI counts more than 1000 but less than the 97th percentile for each cell; (b) gene numbers between 1000 and 7000; (c) percentage of mitochondrial genes < 10%; and (d) percentage of hemoglobin genes <

0.1%. Moreover, we excluded genes expressed in fewer than 3 cells, as well as MALAT1, mitochondrial genes, and hemoglobin genes. And the remaining cells and genes were used for subsequent analysis. Quality control charts are included in SI.4.

Data integration, Dimensionality reduction, and Clustering

After performing quality control and filtering, DoubletFinder v2.0.3 was then employed to identify double cells with an expectation value of doublets calculated as an increase of 0.8% for every 1000 additional cells, pN at 0.25, and pK according to function Find.pk. Library-size normalization was conducted for each cell using the NormalizeData function in Seurat v.4.4.0. The 2000 most variable genes were identified using the FindVariableGenes. Subsequently, all libraries were integrated using Harmony (Ilya Korsunsky et al., 2019) to correct batch effects. ScaleData was applied to regress out variability associated with the numbers of UMIs, followed by dimensionality reduction through RunPCA and RunUMAP (dimensions = 1:20). Finally, clustering of cells was performed using the FindClusters function with a resolution of 0.8 based on the 1:24 dimensions.

Celltype Identifcation

FindAllMarkers was used to compare each cluster to all others to identify canonical cell type-specific marker genes. Each retained marker gene was expressed in a minimum of 25% of cells and at a minimum log fold change threshold of 0.25. The clustering differential expressed genes were considered significant if the adjusted P-value was less than 0.05 and the avg_log_2FC was ≥ 0.25. And the clusters were annotated using cell type-specific signatures and marker genes from Cellmarker2.0 and PanglaoDB.

Differentially Expressed Genes (DEGs) analysis and Enrichment Analysis

233 DEG analysis between cell types was performed following the muscat (v.1.16.0,
234 Crowell et al. 2020) R package pipeline, which facilitates multi-sample, multi-condition
235 comparisons of single-cell RNA-seq data. Genes were ranked by absolute log_2
236 fold-change (log_2FC), and those with p-values > 0.05 (adjusted for multiple
237 comparisons) and log_2FC < 0.25 were removed. Gene Ontology (GO,
238 https://www.geneontology.org/) enrichment analysis of DEGs was implemented by the
239 clusterProfiler R package (Yu et al., 2012). GO terms with corrected P value less than
240 0.05 were considered significantly enriched by DEGs. Kyoto Encyclopedia of Genes
241 and Genomes database (KEGG, http://www.genome.jp/kegg/, Kanehisa et al., 2008)
242 is a database resource for understanding high-level functions and utilities of the
243 biological system, such as cell, organism and ecosystem, from molecular-level
244 information, especially large-scale molecular datasets generated by genome
245 sequencing and other high-through put experimental technologies. We used
246 clusterProfiler R package to test the statistical enrichment of DEGs in KEGG
247 pathways.

248 **Cellular Cross-talk Analysis**

249 We utilized the Cellchat (v.1.6.1, Suoqin Jin et al., 2021, http://www.cellchat.org/) to
250 analyze the expression abundance of ligand–receptor interactions across
251 hippocampal cell types. The analysis was conducted in accordance with the CellChat
252 user guidelines(9). Cell communication networks were inferred by identifying
253 differentially expressed ligands and receptors between distinct hippocampal cell types.
254 Interaction probabilities at the ligand – receptor level were calculated using the default
255 'truncatedMean' method, under which the average expression of a signaling gene is
256 set to zero if it is expressed in less than 10% of cells within a given group. The
257 influence of population size was normalized during the calculation of interaction
258 probabilities. Furthermore, L-R interaction probabilities within each signaling pathway
259 were aggregated to compute pathway-level communication probabilities using the
260 function 'computeCommunProbPathway'. Cell–cell communication networks were
261 subsequently summarized by summing the number of interactions or the previously

calculated communication probabilities via the function ‘aggregateNet’. To compare signaling patterns between METH and Saline groups, we conducted differential expression analysis between METH and Saline samples within each cell type. To ensure consistency in node size and edge weights across inferred networks from different datasets, we calculated the maximum number of cells per cell group and the maximum interaction counts (or interaction weights) across the two datasets. Differential and conserved networks were identified based on their functional roles, and their divergence indicators were computed accordingly. We also compared outgoing, incoming, and overall signaling patterns between the two datasets and across different cell types. To identify major signaling roles of specific cell types within defined pathways, we visualized the computed centrality scores using heatmaps. Discrepant ligands and receptors were identified if both the log-fold change (logFC) and the percentage of cells expressing the gene in a given cluster exceeded 0.1 in either sender or receiver cells, as determined by the function ‘identifyOverExpressedGenes’. Finally, differentially expressed L-R pairs were extracted based on upregulated or downregulated ligands and receptors in METH compared to Saline groups.

Pseudotime analysis

Monocle2(10) (version 2.18.0) was utilized for pseudotime trajectory analysis to elucidate the differentiation trajectory of cell development. The UMI matrix was extracted from the Seurat object and used to create a new object with the ‘newCellDataSet’ function. For the trajectory analysis, the 2000 most highly variable genes were selected, followed by dimensionality reduction with the DDRTree method and cell ordering with the ‘orderCells’ function. Genes exhibiting significant changes along the pseudotime trajectory were identified using the ‘differentialGeneTest’ function. The ‘plot_cell_trajectory’ function was utilized to visualize the trajectory in a two-dimensional space, effectively presenting the cell differentiation state. The observed branching patterns in the single-cell trajectories reflect distinct biological

290 functions, which were inferred based on gene expression dynamics during
291 development.

292 SCENIC analysis

293 SCENIC analysis was utilized to explore key transcription factors (TFs) that
294 regulate inter-cell type differences. The analysis was conducted using pySCENIC with
295 default parameters, following the established protocol(11). Initially, a co-expression
296 network was constructed using GRNBoost2. Subsequently, regulons for each
297 transcription factor were inferred using the RcisTarget motif databases(12)
298 (mm10-refseq-r80-10kb-up-and-down-tss.mc9nr.feather and
299 mm10-refseq-r80-500bp-up-and-100bp-down-tss.mc9nr.feather). Activity scores
300 (AUC values) for each TF regulon in individual cells were calculated using AUCell.
301 Significant TF regulons associated with specific cell types were identified using the
302 'FindAllMarkers' function in Seurat. The regulatory networks involving transcription
303 factors and their target genes were further visualized and analyzed using Cytoscape
304 (v3.10.1). Additionally, functional enrichment analyses of the target genes were
305 conducted using the clusterProfiler R package, as previously described.

306 Statistical Analysis

307 For the experimental data, statistical analyses and graphical visualization were
308 performed using GraphPad Prism software (version 8.0.2, USA). The normality of
309 data distribution was assessed using the Shapiro–Wilk test, although the sample
310 size in each group was close to 30, which is considered relatively large. Results from
311 the Y-maze and NOR tests were presented as mean ± SEM. Between-group
312 differences in the alternation triplet of the Y-maze, as well as the discriminant index,
313 preference index, total exploration time, and frequency of interactions with new and
314 old objects within 10 minutes, were analyzed using the unpaired Student's t-test. A P
315 value < 0.05 was considered statistically significant, and all statistical tests were
316 two-tailed.

For the single-cell RNA sequencing data, statistical analyses and figure generation were conducted using R (v4.3.1). Bioinformatic tools were applied to analyze cellular clustering, differentially expressed genes, functional enrichment, intercellular signaling cross-talk, single-cell trajectory inference, and SCENIC-based regulatory network analysis.

322 # Result

323 ## 1. Chronic METH exposure led to cognitive decline in adult mice.

324 The construction of the METH chronic exposure mouse model and the
325 arrangement of behavioral experiments are illustrated in Fig.1.A. Adult male mice
326 subjected to chronic METH exposure exhibited significant declines in working memory
327 and spatial cognition, as demonstrated by Y-maze tests conducted at the end of both
328 the second and fourth weeks of administration. In the 2-week test, the mean
329 difference between the METH-treated (n=32) and saline-treated (n=29) groups was
330 -0.1664 (95% CI: -0.2126 to -0.1202, $p < 0.0001$). In the 4-week test, the mean
331 difference was -0.2202 (METH, n=30 vs. Saline, n=29; 95% CI: -0.2728 to -0.1676, p
332 < 0.0001) (Fig.1B).

333 Following chronic METH exposure, NOR tests also revealed impairments in the
334 animals' ability to discriminate novel objects. In the 2-week NOR test, the
335 discrimination index was 0.3119 ± 0.0300 (mean ± SEM) for saline-treated mice
336 (n = 29), compared to 0.1569 ± 0.0462 for METH-treated mice (n = 29). The mean
337 difference in discrimination index between the METH and Saline groups was -0.1550
338 ± 0.0551 (p = 0.0068, 95% CI: -0.2653 to -0.0446) (Fig.1C). The preference index
339 was 0.6559 ± 0.0150 for saline-treated mice and 0.5785 ± 0.0231 for
340 METH-treated mice, resulting in a mean difference of -0.07748 ± 0.0276 (p =
341 0.0068, 95% CI: -0.1327 to -0.0223) (Fig.1C).

342 The total exploration time for novel objects was 28.36 ± 2.285 seconds in the
343 saline group, compared to 18.38 ± 1.453 seconds in the METH-treated group. The
344 mean difference in total exploration time for novel objects was -9.974 ± 2.708 (p =
345 0.0005). For old objects, the total exploration time was 14.79 ± 1.173 seconds in the
346 saline group and 13.44 ± 1.067 seconds in the METH group, yielding a mean
347 difference of -1.352 ± 1.586 (p = 0.3976) (Fig.1D).

348 Exploration frequency analysis showed that saline-treated mice explored the
349 novel object an average of 25.55 ± 1.565 times, compared to 19.66 ± 1.368 times

in the METH group. The mean difference in novel object exploration frequency was -5.897 ± 2.079 (p = 0.0063) (Fig.1E). Similarly, the frequency of old object exploration was 19.14 ± 1.359 in the saline group versus 15.41 ± 1.010 in the METH group, with a mean difference of -3.724 ± 1.693 (p = 0.0320) (Fig.1E).

Collectively, these findings indicate that following 2 weeks of METH treatment, mice exhibited significant impairments in cognitive and mnemonic functions, as well as reduced exploratory behavior.

In the 4-week NOR test, the discrimination index was 0.3019 ± 0.0389 for the saline group (n = 29), compared to 0.0880 ± 0.0368 for the METH group (n = 29). The mean difference in discrimination index between the METH and saline groups was -0.2139 ± 0.0536 (p = 0.0002, 95% CI: -0.3213 to -0.1066) (Fig.1F). The preference index was 0.6510 ± 0.0195 in the saline group and 0.5440 ± 0.0184 in the METH group, resulting in a mean difference of -0.1070 ± 0.0268 (p = 0.0002, 95% CI: -0.1606 to -0.0533) (Fig.1F).

The total exploration time for novel objects was 20.04 ± 1.502 seconds in the saline group and 13.05 ± 1.019 seconds in the METH group, yielding a mean difference of -6.996 ± 1.815 (p = 0.0003) (Fig.1G). For old objects, the total exploration time was 10.50 ± 0.919 seconds in the saline group and 11.39 ± 1.119 seconds in the METH group, with a mean difference of 0.8922 ± 1.448 (p = 0.5402) (Fig.1G).

Exploration frequency for novel objects was 22.10 ± 1.293 in the saline group and 18.52 ± 1.521 in the METH group, resulting in a mean difference of -3.586 ± 1.996 (p = 0.0778) (Fig.1H). For old objects, the exploration frequency was 18.10 ± 1.658 in the saline group and 15.03 ± 1.585 in the METH group, with a mean difference of -3.069 ± 2.294 (p = 0.1864) (Fig.1H).

These findings indicate that chronic METH exposure leads to a decline in learning and cognitive memory abilities in mice. Although no significant differences in exploration frequency were observed between the METH and saline groups during the 4-week test, the discrimination and preference indexes showed greater statistical significance and further deterioration in the METH group compared to the 2-week test.

These results suggest that prolonged METH exposure may progressively impair cognitive function.

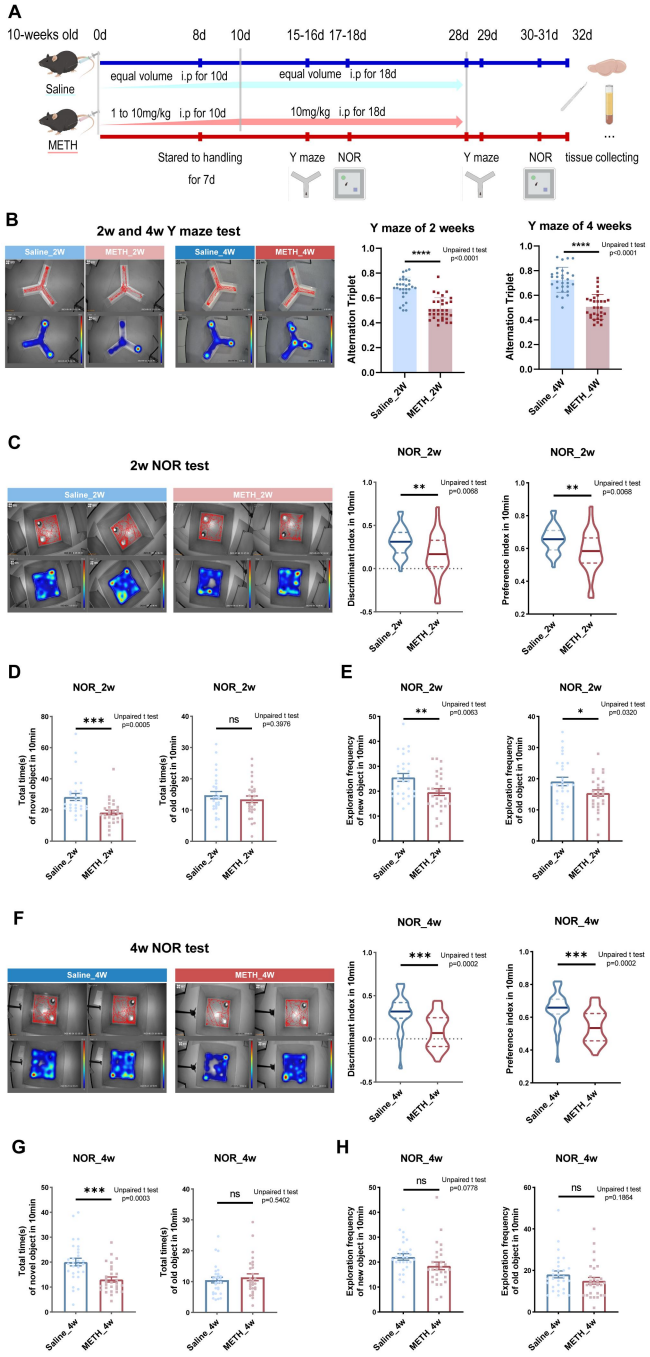

Fig.1. Mice treatment and result of behaviour tests. (A) The construction mouse model of chronic METH abuse. (B) The track visualizations and heatmaps of Y maze in 2 and 4 weeks. (C) The track visualizations, heatmaps and the discrimination and preference index of 2 weeks NOR test. (D-E) The total exploration time and frequency of familiar or novel objects of 2 weeks NOR test. (F) The track visualizations, heatmaps and the discrimination and preference index of 4 weeks NOR test. (G-H) The

total exploration time and frequency of familiar or novel objects of 4 weeks NOR test. Asterisks indicate statistical significance (*$p < 0.05$; **$p < 0.01$; ***$p < 0.001$; ****$p < 0.0001$). All data are presented as mean ± SEM.

2. Identification of hippocampal cell clusters in mice with chronic METH exposure.

To investigate the impact of chronic METH abuse, single-cell RNA-seq was performed on the hippocampi of mice treated with either saline or METH. A total of 60,549 high-quality cells were obtained after stringent quality filtering, including 31,219 cells from saline-treated mice and 29,330 cells from METH-treated mice. Clustering analysis was then conducted based on gene expression profiles using cluster-specific variable genes, following the Seurat pipeline (logfc.threshold = 0.25, min.pct = 0.25). Subsequently, Uniform Manifold Approximation and Projection (UMAP) analysis at a resolution of 0.8 identified a total of 31 distinct transcriptional clusters in each experimental group (Fig.2.A). Using established hippocampal markers from databases (primarily CellMarker2.0 and PanglaoDB), we annotated 18 distinct cell types within the hippocampus. These included astrocytes (cluster 6 and 27, marked by *Aqp4*, *Gfap*, *Gja1*, and *Slc1a3*), Cajal-Retzius cells (cluster 14, marked by *Cntnap2*, *Reln*, *Clstn2*, and *Kcnh7*), Cldn5^{+} and Cldn5^{-} mural cells (cluster 9 and 11, marked by *Vtn*, *Pdgfrb*, *Rgs5*, and *Atp13a5*, distinguished by high or low expression of *Cldn5*), endothelial cells (cluster 4, 7, 8, 10, and 16, marked by *Cldn5*, *Flt1*, *Pecam1*, and *Kdr*), ependymal cells (cluster 23, marked by *Ccdc153*, *Tmem212*, *Rarres2*, and *Mia*), fibroblasts (cluster 25, marked by *Dcn*, *Spp1*, *Nupr1*, and *Igfbp2*), macrophages (cluster 12, marked by *Pf4*, *Mrc1*, *F13a1*, and *Lyz2*), microglia (cluster 0, 1, 3, 21, and 29, marked by *Tmem119*, *Cx3cr1*, *P2ry12*, and *Aif1*), neurons or neuroblasts (cluster 17, marked by *Igfbpl1*, *Sox11*, *Fabp7*, and *Nnat*), neutrophils (cluster 26, marked by *S100a9*, *Retnlg*, *G0s2*, and *Slpi*), NK-T cells (cluster 19, marked by *Ccl5*, *Trbc2*, *Cd3g*, and *Ms4a4b*), neural stem cells (NSCs, cluster 20, marked by *Clu*, *Aldoc*, *Cpe*, and *Hopx*), neurons derived from NSCs (cluster 22,

417 marked by *Chchd10*, *Pcp4*, *Fxyd1*, and *Ppp1r1b*), oligodendrocytes (cluster 2, 5, 24,
418 28, and 30, marked by *Mbp*, *Mog*, *Cldn11*, and *Mag*; cluster 24 was identified as
419 perivascular oligodendrocytes), oligodendrocyte precursor cells (cluster 13, marked
420 by *Pdgfra*, *Cacng4*, *Sox10*, and *Cspg4*), smooth muscle cells (cluster 15, marked by
421 *Acta2*, *Myl9*, *Tagln*, and *Myh11*), and T cells (cluster 18, marked by *Cd44*, *Cd52*, *Cd74*,
422 and *Plac8*). The top four highly expressed genes for each cluster are displayed
423 (Fig.2.B&D, SI.1). These findings indicate that, in addition to neurons, the
424 hippocampus comprises a diverse array of cell types, including neuroglia, stromal
425 cells, vascular cells, and immune cells, forming a complex yet highly organized
426 microenvironment. Within this microenvironment, METH exerts widespread effects
427 across multiple cell types, potentially contributing to impairments in learning and
428 memory. This knowledge may help elucidate the characteristics and functional
429 alterations of specific hippocampal cell types under chronic METH exposure.

430 Following clustering analyses, cell proportion analysis revealed that chronic
431 METH exposure led to a decrease in the proportion of astrocytes from 6.6% to 5.5%,
432 endothelial cells from 24.3% to 22.5%, smooth muscle cells from 1.0% to 0.6%,
433 oligodendrocyte precursor cells from 1.6% to 1.0%, neutrophils from 0.3% to 0.1%,
434 ependymal cells from 0.4% to 0.3%, and fibroblasts from 0.3% to 0.2%. Conversely,
435 an increase was observed in the proportion of microglia from 36.0% to 39.8%, NK-T
436 cells from 0.5% to 0.7%, and neurons derived from NSCs from 0.2% to 0.6% (Fig.
437 2.C).

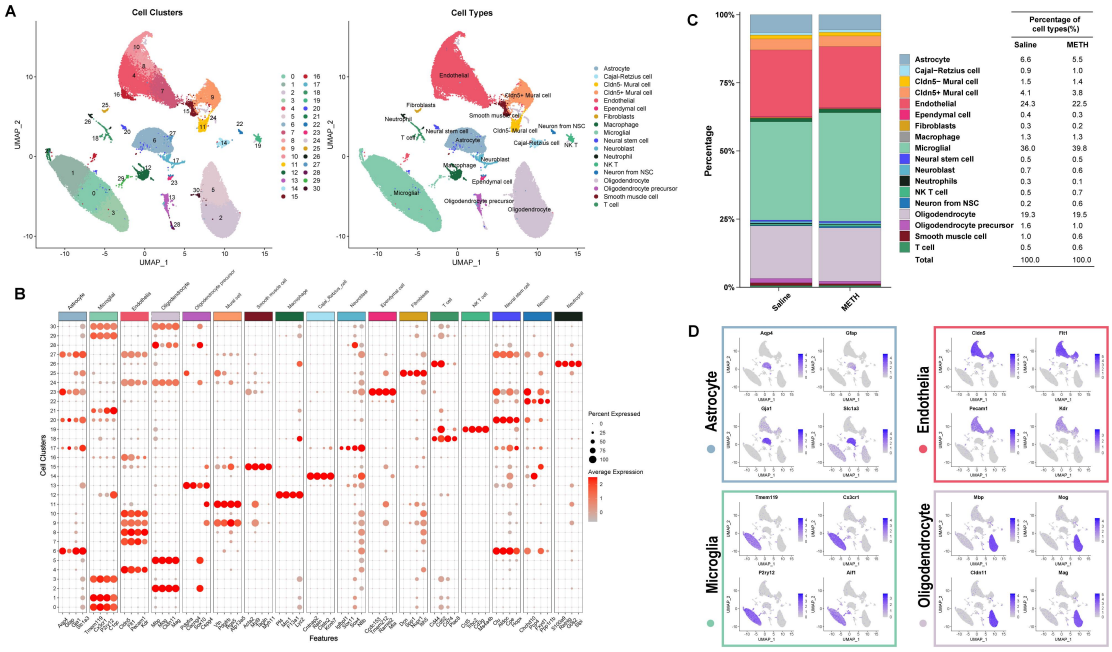

Fig.2. Hippocampus cell clusters of saline and METH mice. (A) The Umap-distributed plots showing 31 hippocampal cell clusters in saline and METH groups. (B) The average expression of known marker genes of hippocampal clusters. (C) The percentage of cells in hippocampal clusters in saline and METH groups. (D) The marker genes expression's featureplots of astrocyte, endothelia, microglia and oligodendrocyte.

3. Chronic METH exposure induced gene and function changes of hippocampal cells in mice.

Chronic METH abuse elicits a diverse array of cellular responses, ultimately resulting in multifactorial cognitive decline. To elucidate the underlying mechanisms of this cognitive impairment, we employed muscat — a pseudobulk-based analytical framework — for multi-sample, multi-condition, cluster-specific differential gene expression analysis, enabling the identification of differentially expressed genes (DEGs) within each cell cluster. Strikingly, most DEGs were found to be specific to individual cell types following chronic METH exposure. For example, Cldn5^{+} mural cells exhibited the highest number of DEGs, with 679 identified (368 upregulated and 311 downregulated) (Fig.3.A), including 336 cell type-specific DEGs (Fig.3.B).

456 Similarly, endothelial cells showed 565 DEGs (322 upregulated and 243
457 downregulated) (Fig.3.A), of which 268 were cell type-specific. Notably, a subset of
458 116 DEGs was shared between these two cell types (Fig.3.B).

459 These DEGs were subsequently categorized based on their direction of
460 regulation (upregulated or downregulated) and subjected individually to pathway
461 enrichment analysis using Gene Ontology (GO), in order to elucidate their functional
462 roles and the molecular basis of METH-induced cognitive decline. The upregulated
463 and downregulated Biological Processes (BP) from the GO analysis are presented
464 (Fig.3.C – F and SI.2). Moreover, analysis of cell type-specific enrichment patterns
465 revealed that, in addition to distinct functional effects, there exist complex
466 co-regulatory mechanisms across different cell types in response to chronic METH
467 exposure.

468 Neuroinflammation is a complex process that can be triggered by various factors,
469 such as exposure to toxic substances like METH. METH-induced neuronopathies, in
470 particular, have been found to constantly produce a range of impact factors and cells'
471 changes that contribute to the exacerbation of neuroinflammation. Microglia up
472 regulates immunoprotein receptor genes (such as *Fcer1g*, *Fcgr3* and *Il1rl2*) to
473 enhance immune sigal reception and cell chemotaxis (*Ccl2*, *Cxcl14*, *Trpv4*, et al.)
474 (Fig.3.E). Astrocytes enhance their capacity for gliogenesis and migration through the
475 expression of key regulatory genes (*P2ry12*, *Rras*, *Efemp1*,et al.) thereby modulating
476 the inflammatory response via the NF-κB signaling pathway (involves *Tnfaip6*,
477 *Nfkb1*,*Nfkbia*) (Fig.3.C). In addition to the responses of neurogliocytes, genes like *Grn*
478 and *Trem2* (associated with astrocye and microglia activation) are up-regrated in both
479 microglia and T cell, suggesting potential communication between central resident
480 and peripheral immune cells, which may jointly participate in the neuroinflammatory
481 response. T and NK-T cells become more active in leukocyte or lymphocyte mediated
482 immunity, but T cells active by complement-mediation (*C1qb*, *C1qc*, *C1qa*, *Trem2*)
483 while NK-T cells depend more on reception of cytokines (*Il18r1*, *Fcer1g*) or
484 recognition of receptors on membrane (*Itgb2*, *Ptprc*, *Tyrobp*,et al.). However

485 neutrophils down-regulate chemokine-mediated signaling pathway (*Cxcr4*, *Ccl3*, *Ccl4*)
486 that may indicates neuroinflammation changes from acute (leukocyte-leading) to
487 chronic (lymphocyte-leading). Macrophage also weaken leukocyte activation (*Cd28*,
488 *Itgam*, *Il18*, *Tnfsf9*, et al.) but strengthen T cell activation.

489 The maintenance of a stable neural microenvironment relies on a healthy
490 blood-brain barrier (BBB) system(13). METH can induce structure and function
491 disruptions in the BBB, although its chronic effects remain uncertain. In our study, we
492 observe that endothelial cells upregulate detoxification funtions (*Gstm1*, *Abcg2*, *Fbln5*,
493 et al.) and autophagy-related genes (*Qsox1*, *Fnbp1l*, *Trp53inp1*, et al.), while
494 downregulating angiogenesis-associated genes (*Hipk2*, *Tnfrsf1a*, *Vegfc*, *Cldn5*, et al.)
495 and cell-cell adhesion molecules (*Hmcn1*, *Ceacam1*, *Cdh10*, et al.).
496 Furthermore,endothelial dysfunction is also implicated in learning or memory deficits
497 and cognitive impairments (*Dbi*, *Bche*, *Psen2*, *Prnp*, et al.) as well as nervous system
498 development (*Macf1*, *Ptprz1*, *Vegfc*, *Ctnnb1*, et al.) suggesting an interplay between
499 neuronal activities and vascular functions (Fig.3.D). Similarly,dysfunctions in *Cldn5*$^{+}$
500 mural cells are associated with altered vascular permeability (*Ctnnbip1*, *Pde3a*,
501 *Ceacam1*, *Cldn5*) and developmental processes (*Atp2b4*, *Sfrp2*, *Vegfc*, *Tgfbr2*, et al.),
502 as well as cognitive impairments (*Psen2*, *Bche*, *Nf1*, *Prkn*, et al.), and increased
503 autophagic cell death (*Bmf*, *Bnip3*, *Lamp1*, *Cdkn2d*) after METH trearment. As a
504 structure of arteriole in hippocampus, SMCs exhibit suppressed inflammatory
505 responses such as leukocyte migration (*Abl2*, *Fcer1g*, *Vcam1*, *Icam1*, et al.), glial cell
506 activation (*Syt11*, *C1qa*, *Cx3cr1*, *Trem2*, et al.) and IL-6 production (*Dhx9*, *Fcer1g*,
507 *Syt11*, *Il6ra*).

508 The response of BBB cell types to METH is heterogeneous(14). In our data,
509 within the Wnt signaling pathway—which promotes angiogenesis and vascular
510 remodeling(15)—both *Cldn5*$^{+}$ and *Cldn5*$^{-}$ mural cells show downregulation through
511 distinct sets of DEGs, whereas endothelial cells exhibit upregulation of this pathway.
512 Cell-substrate adhesion is enhanced in mural cells and SMCs, but reduced in ECs.

513 Although this ultimately results in increased BBB permeability, the underlying
514 mechanisms differ between the inner and outer layers of the vasculature.

515 Metabolite shuttling and extracellular vesicle signaling provided by
516 oligodendrocytes are essential for the normal functioning of neurons, particularly their
517 axons(16). In our study, we observed significant changes in the metabolic status of
518 oligodendrocytes (Fig.3.F), including alterations in organic acid biosynthesis
519 (*Cyp27a1*, *Per2*, *Glul*, et al.), amino acid metabolic (*Glul*, *Bcat1*, *Hmgcll1*, et al.),
520 glycolipid metabolic process (*Pikfyve*, *Pigc*, *Pnpla7*, et al.) and other processes.
521 Additionally, METH influences neural structure and function-related changes such as
522 axonogenesis (GO terms:axonogenesis, postsynapse organization, central nervous
523 system neuron development, et al.) and synaptic vesicle signaling (GO terms:
524 vesicle-mediated transport in synapse, synaptic vesicle recycling, vesicle localization,
525 et al.), which are partially upregulated or downregulated. Furthermore,
526 oligodendrocyte precursor cells exhibit negative effects on cell development and
527 synaptic plasticity while also increasing neuroinflammation response to DNA damage
528 stimulus. These effects may contribute to neuronal dysfunction and ultimately lead to
529 cognitive decline. Astrocytes play a vital role in supporting neuronal function
530 throughout the central nervous system by regulating synapse development and
531 neurotransmitter release at synapses while providing adequate energy supply and
532 modulating information processing within neurons(17). During chronic METH abuse,
533 astrocytes downregulate bioprocesses involved in translation and metabolism
534 (Fig.3.C), such as translation at synapse (*Rpl12*, *Rpl35*, *Rps26*, et al.) and the
535 generation of precursor metabolites and energy (*Adh5*, *Ndufa5*, *Bpgm*, et al.), which
536 may impede normal neurotransmitter vesicle transmission. Simultaneously, astrocytes
537 enhance bioprocesses related to multiple inorganic cation transportation including
538 potassium (*P2ry12*, *Kcnd3*, *Slc24a2*, et al.), sodium (*Slc24a2*, *Nkain1*, *Hcn2*, et al.), or
539 calcium (*P2ry12*, *Tmem38a*, *Slc24a4*), which may interfere regulation of neural
540 membrane potential. However, we also observe that astrocytes have positive effects
541 of neuron projection extension (*Nrp2*, *Rtn4*, *Jade2*, et al.), axon ensheathment (*Abca2*,

542 *Mal*, *Ugt8a*, et al.), or oligodendrocyte differentiation (*Abca2*, *Mal*, *Mag*, et al.). These
543 results may imply that astroctyes have dfferent subsets performing diverse functions
544 according to their positions and cellular contacts in hippocampus.

545 Adult hippocampal neurogenesis (AHN) is a complex and dynamic
546 developmental process regulated by a multitude of factors. It involves a sequential
547 progression from neural stem cells (NSCs), through radial glia-like cells and
548 neuroblasts, to fully differentiated mature neurons. This process plays a crucial role in
549 cognitive functions such as learning, memory formation, and emotional regulation.
550 Furthermore, alterations in AHN have been associated with memory impairments,
551 highlighting its significance in maintaining hippocampal plasticity and overall brain
552 function(18). At the initiation of adult hippocampal neurogenesis (AHN), we observe
553 that neural stem cells (NSCs) downregulate pathways related to the generation of
554 precursor metabolites and energy (e.g., *Sdhaf4*, *Nduf* family, *Uqcrh*, *Gapdh*),
555 suggesting that METH may impair the proliferation and differentiation potential of
556 NSCs. Furthermore, METH induces endoplasmic reticulum stress (e.g., *Tmco1*, *Atf3*,
557 *Hspa5*, *Gsk3b*), activates apoptotic processes (e.g., *Btg2*, *Prnp*, *Cebpb*, *Ctsz*), and
558 promotes autophagy (e.g., *Ddrgk1*, *Ctsa*, *Mcl1*, *Sh3glb1*) in NSCs. These alterations
559 consequently lead to increased expression of β-amyloid-related genes (e.g., *Prnp*,
560 *Apoe*, *Psenen*, *Rtn4*) and IL-6-related genes (e.g., *Ncl*, *Fcer1g*, *Il1a*, *Lbp*), which may
561 trigger neuroinflammatory responses. Adult NSC activation in mice is known to be
562 regulated by circadian rhythms and intracellular calcium dynamics(19). In our
563 dataset, astrocytes from METH-treated mice show enhanced expression of circadian
564 rhythm-related genes (e.g., *Per2*, *Ptgds*, *Ciart*, *Id3*), calcium-mediated signaling
565 pathways (as previously mentioned), and genes involved in the regulation of
566 neurogenesis (e.g., *Per2*, *Mag*, *Fbxo31*, *Slc7a5*). These findings suggest that
567 astrocytes may attempt to compensate for METH-induced damage by activating
568 NSCs; however, this compensatory mechanism could accelerate the depletion of the
569 NSC pool.

570 During the neuroblast stage, METH exposure increases oxidative stress through
571 upregulation of genes associated with oxidative stress response (e.g., *Setx*, *Prkra*,
572 *Agap3*, *Lig1*) and alters DNA regulatory mechanisms involved in cell division (e.g.,
573 *Ciz1*, *Rpa2*, *Mcm7*, *Ssbp1*). Additionally, METH suppresses cell-substrate adhesion
574 by downregulating genes such as *Myoc*, *Ccn1*, *Ptn*, and *Lrp1*. As the remaining
575 neuroblasts mature into neurons, METH exerts more pronounced effects, resulting in
576 a higher number of DEGs. Under METH exposure, neurons derived from NSCs
577 upregulate pathways related to endoplasmic reticulum stress (e.g., *Tmco1*, *Atf3*,
578 *Hspa5*, *Pdia3*), TNF superfamily cytokine production (e.g., *Ncl*, *Fcer1g*, *Il1a*, *Lbp*),
579 neuron death (e.g., *Prnp*, *Ctsz*, *Mcl1*, *Jun*), leukocyte chemotaxis (e.g., *Fcer1g*, *Lbp*,
580 *Cxcl10*, *Hmgb1*), and β-amyloid metabolic processes (e.g., *Prnp*, *Apoe*, *Psenen*,
581 *Rtn4*). Simultaneously, these neurons downregulate key pathways involved in energy
582 metabolism (e.g., *Sdhaf4*, *Nduf* family, *Cycs*, *Gapdh*) and mitochondrial structure and
583 function (e.g., *Slc25a* family, *Vdac1*, *Atpif1*, *Acaa2*).

584 Cajal-Retzius cells (CRs) are transient neurons that almost completely disappear
585 in the neocortex after birth but survive up to adulthood in the hippocampus at a certain
586 percentage. CRs are synaptically integrated into hippocampal circuits relating to
587 hippocampal-related behaviors and network. Abnormal survival of CRs has been
588 linked to deficits in adult neuronal and cognitive functions(20, 21). In our analysis, CRs
589 down-regulate various neural growth and maturation-relevant processes including
590 axon extension (e.g.,*Sema6d*, *Dclk1*, *Cttn*, *Sin3a*), dendrite genesis (e.g., *Nlgn1*,
591 *Dclk1*, *Farp1*, *Il1rapl1*), synapse organization (e.g., Lrrtm4, Lhfpl4, Farp1, Mark2) and
592 neuron migration (e.g., *Nr4a2*, *Dclk1*, *Sema6a*, *Mark2*, *Cdkl5*).

593 In summary, METH exerts direct neurotoxic effects on NSCs and their
594 developmental trajectory, while also indirectly disrupting the function of
595 neurogenesis-supporting cells, ultimately contributing to cognitive decline.

596 Ependymal cells, a type of neuroglia that provides support to neurons, form the
597 epithelial lining of the brain ventricles(22). METH exposure induces significant

changes in ependymal cells, including the upregulation of genes associated with cilium organization and motility (e.g.,*Meig1*, *Cfap* family, *Lca5*, *Tmem216*), suggesting enhanced cerebrospinal fluid circulation and a potential compensatory response to toxic substances by facilitating the clearance of harmful molecules. However, METH also downregulates genes involved in intracellular transport (e.g., *Ptpn14*, *Pdcd10*, *Txn1*, *Sorl1*) and protein processing (e.g., *Gsn*, *Txn1*, *Tmsb10*, *Sorl1*), indicating impaired cellular functions that may compromise ependymal cell homeostasis.

Fibroblasts, which originate from embryonic mesenchymal cells, perform a variety of complex and diverse functions in the hippocampus, including extracellular matrix (ECM) homeostasis, secretome regulation, mechanosensation, progenitor cell activity, and immune modulation(23). However, their specific roles in this brain region remain incompletely understood. Compared to the saline group, METH-treated fibroblasts exhibit increased expression of genes associated with responses to metal ions (e.g., *Gsn*, *Mt2*, *Mt1*, *Id2*, *Hnrnpa1*) and toxic substances (e.g., *Gstm1*, *Inmt*, *Mt2*, *Mt1*), as well as markers linked to astrocyte differentiation (e.g., *Vim*, *Plpp3*, *Sox9*, *Id2*). Notably, downregulation of the JNK and MAPK signaling pathways (e.g., *Map4k4*, *Sh3rf1*, *Ccn2*, *Gadd45b*, *Dab2*) is associated with reduced fibrosis, suggesting that fibroblasts may undergo functional transitions—from stress responses such as cell death and inflammation—to roles in cellular support and transformation.

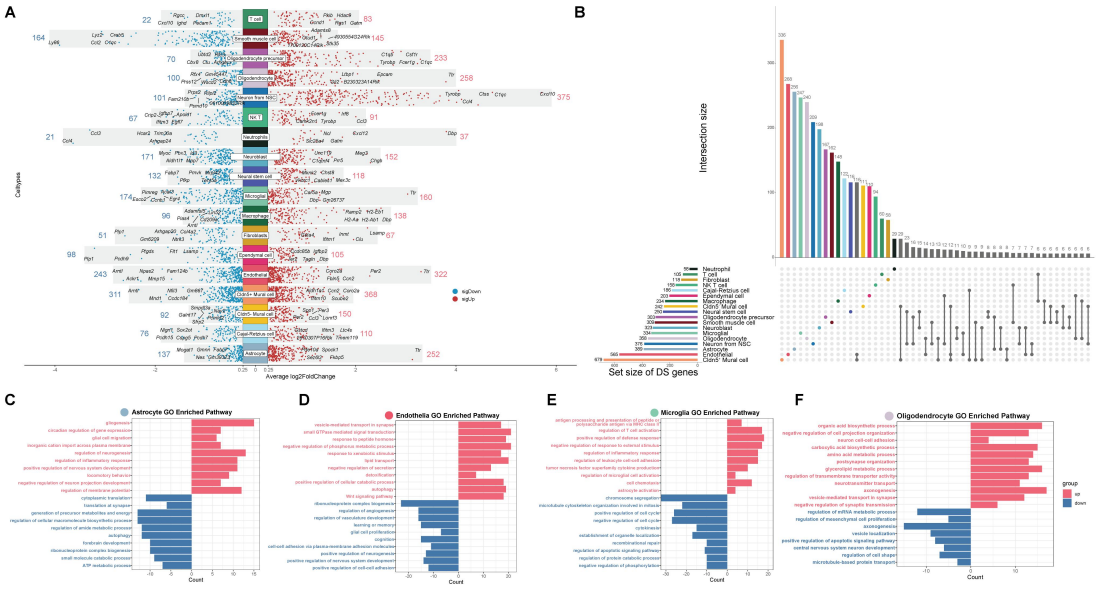

618 Fig.3. Differentally expressed genes(DEGs) induced by chronic METH exposure in hippocampal cell
619 types. (A) The manhattanplot showing the number of DEGs in each hippocampal cell types(METH v.s.
620 saline), the red dots and number represented for up-regulated genes and the blue ones represented for
621 down-regulated genes. (B) The upset plot showing the number of all of unique and some of shared genes
622 of hippocampal cell types. (C-F) The biocprocess in GO terms enriched separately by up or
623 down-regulated genes of astrocyte, endothelia, microglia and oligodendrocyte. Criteria for DEGs by
624 Muscat: p_value < 0.05, abs(log2FC) > 0.25).

625

626 4. METH-induced alterations of crosstalk between cell types in 627 hippocampus led to hippocampal environment disturbance.

628 Considering the neurotoxic effects of METH on various cell types in the
629 hippocampus and its intricate impact, we conducted an investigation into hippocampal
630 intercellular communication to elucidate the role of these interactions in cognitive
631 decline. Our findings reveal a slight increase in both the total number of cell
632 communication interactions (from 18,396 to 19,054) and their strength (from 0.883 to
633 0.841) following METH treatment (Fig.4.A). The results demonstrate that chronic
634 METH abuse induces a greater diversity of changes in the differential number of
635 interactions among cell types compared to changes in interaction strength (Fig.4.B
636 and C). For instance, astrocytes mildly enhance the number of interactions with mural
637 cells, ECs, and OPCs but decrease the strength of these interactions, suggesting
638 reduced efficacy of communication signals under METH influence. Neuron derived
639 from NSCs increase the number of interactions with most cell types while exhibiting
640 minimal changes in interaction strength, which corresponds to the up-regulation of
641 TNF superfamily cytokines and damage signals associated with ER stress or
642 amyloid-beta mentioned in DEGs analysis. In association with neuroinflammatory
643 response, microglia significantly augment their own interaction strength, potentially
644 contributing to neuroinflammation.

From the perspective of cellular communication patterns (incoming and outgoing), hippocampal cells treated with METH exhibit 4 incoming patterns similar to the Saline groups, primarily related to microglial activation, BBB function, neural development, and immunity (Fig.4.D). However, in terms of outgoing patterns, the communication patterns of METH groups are divided into 8 distinct patterns compared to 5 in the Saline group. These outcoming patterns mainly involve microglia activation, endothelial cell signaling, neural development processes, immune responses, as well as a mixed pattern reflecting changes in the neural microenvironment (Fig.4.E). The disruption caused by METH results in confusion within cellular crosstalk specifically through disturbances in outcoming communication pathways within the hippocampus. To further elucidate how METH affects cellular communication networks concretely, we conducted an analysis focusing on specific signal pathway alterations. By calculating Euclidean distance (Fig.4.F), we identified several key differential functions between METH and Saline groups: RANKL (Receptor Activator of Nuclear Factor-κ B Ligand, belongs to tumor necrosis factor (ligand) superfamily, also proteinically known as TNF-related activation-induced cytokine), SELPLG (proteinically known as p-selectin, involving in leukocyte and microglia activation(24)), and CD46 (proteinically known as complement regulatory protein, as a membrane cofactor mediated cleavage cofactor of C3b and C4b, which is a key regulator of classical and selective complement activation cascade, as well as inflammation(25)). We then compared overall information flow across each signal path to determine conservative and METH-specific signaling pathways (Fig.4.G). Additionally，we also examined changes occurring within each outgoing or incoming signal pathway for individual cell types (Fig.4.H).

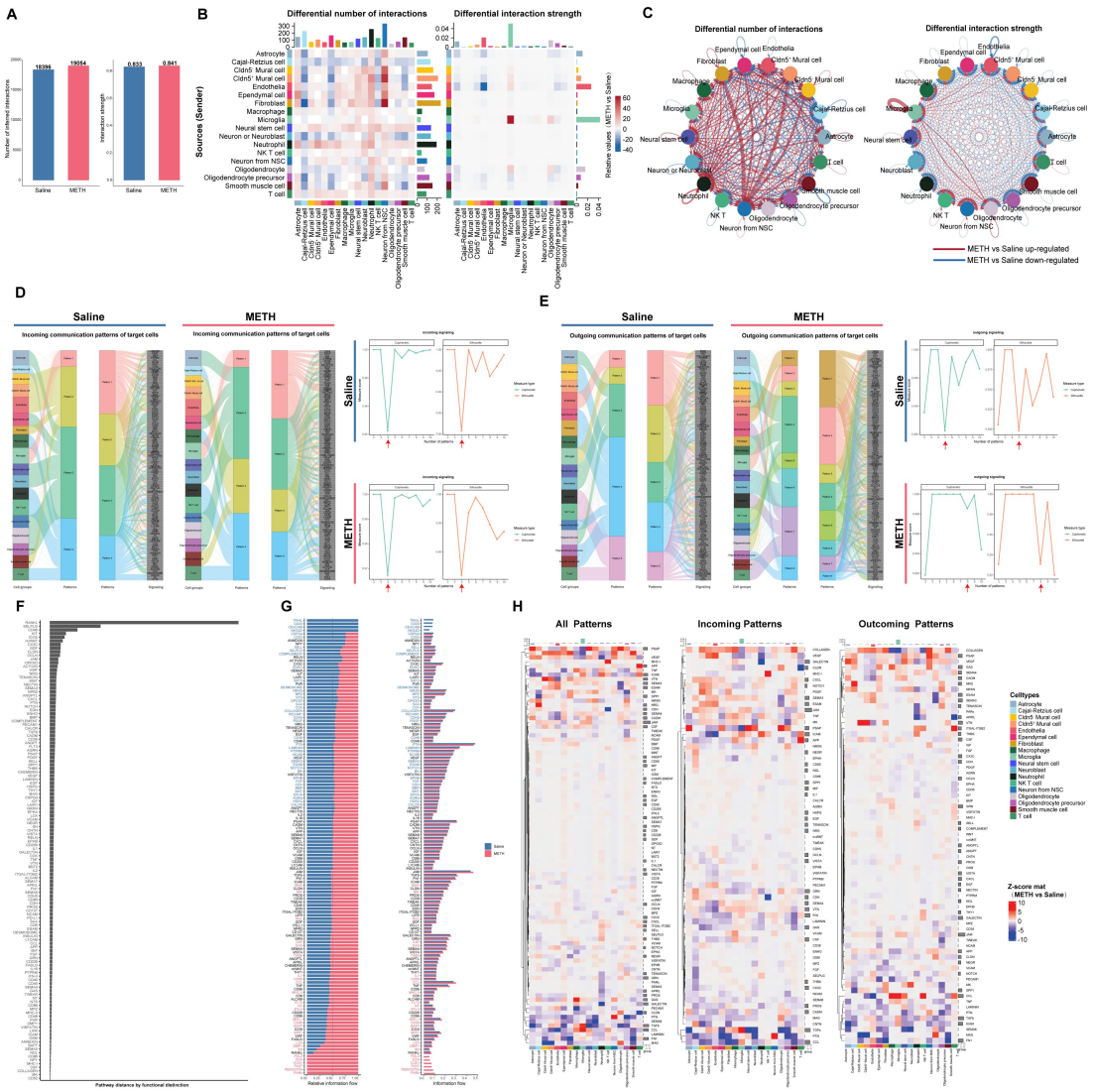

Fig.4. Hippocampal cell types crosstalk alterations induced by chronic METH treatment. (A) The total number of cell communication interactions and the intensity of interactions in saline and METH groups. (B-C) The comparison of the number and the strength of interactions of each cell types between METH and saline groups. (D-E) The incoming and outgoing communication patterns of secreting cells of each groups and the inflection point parameter in clustering algorithm. (F) The identificaton of signaling networks with large (or small) differences according to the Euclidean distance in a shared two-dimensional space. (G) The comparison of the overall information flow of each signal path between two groups. (H) Heatmap showing the incoming, outgoing and all communicated informations' comparison of each signal of each cell type.

680 **5. Pseudo-time series analysis revealed that METH caused changes in**
681 **hippocampal neurogenesis in mice.**

682 Adult neurogenesis in the dentate gyrus of the hippocampus plays a crucial role
683 in cognitive function in mice and is influenced by the local microenvironment or
684 niche(26). However, limited evidence exists regarding the impact of METH exposure
685 on the capacity of NSCs to differentiate into neurons, astrocytes, oligodendrocytes,
686 and other cell types. To address this, we conducted pseudotime analysis to explore
687 how chronic METH exposure affects NSC differentiation trajectories.

688 Along the temporal axis, with NSCs as the starting point, we observed that under
689 normal conditions (Saline group), NSCs (cluster 20) predominantly differentiated into
690 neuroblasts (cluster 17) compared to astrocytes (clusters 6 and 27), following a typical
691 neural developmental trajectory (Fig.5.A). In contrast, METH exposure disrupted this
692 pattern, showing an increased tendency for NSCs to differentiate into astrocytes
693 rather than neuroblasts (Fig.5.D), suggesting impaired neurogenesis.

694 Our analysis reveals that the altered neural developmental trajectory in the
695 METH group is associated with changes in the expression of genes such as Bsg, Ccl4,
696 Fos, and Sox11 (Fig.5.F), as illustrated by other differentially expressed genes in the
697 heatmap (Fig.5.E). In contrast, normal developmental progression from NSCs to
698 neuroblasts is more closely associated with the expression of Flt1, Hspb1, Igfbp7,
699 Tmsb10, and other related genes (Fig.5.B and C).

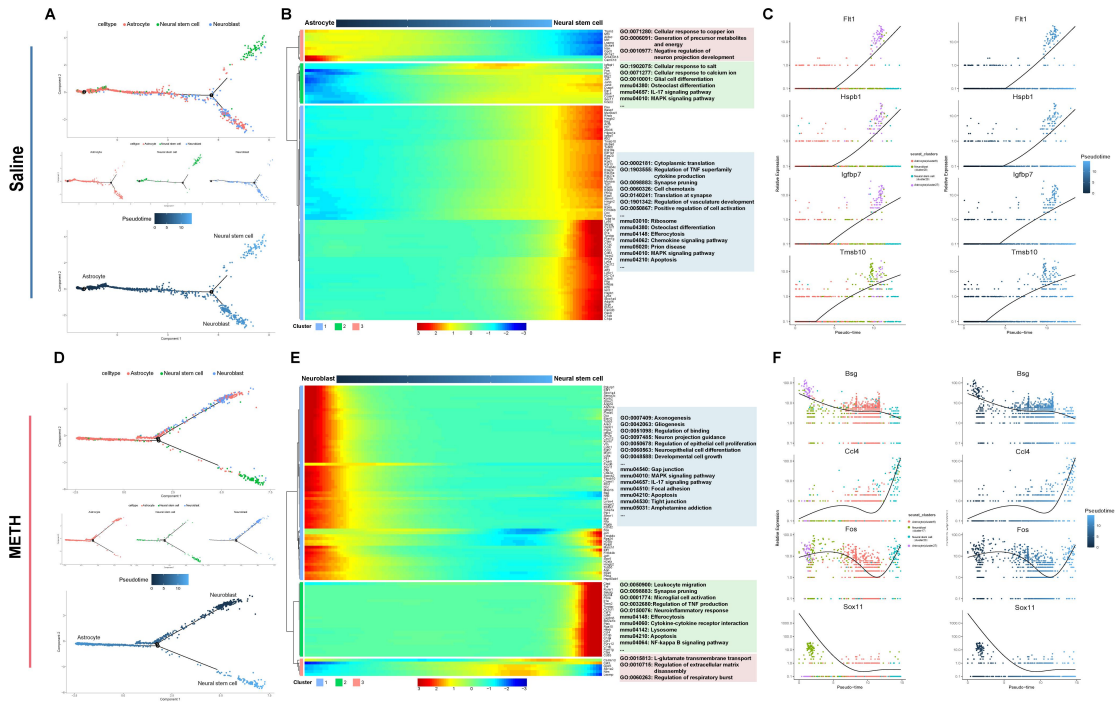

Fig.5. The development direction of hippocampal neural stem cells and the regeneration of hippocampal nerve were analyzed in pseudo-time series. (A, C) The pseudo temporal differentiation locus of neural stem cells, astrocytes and neuroblasts in saline (A) or METH (C) group. (B, D) Heatmap showing the expression of specific genes(rows) in subclusters (columns) along the maturation trajectory from neural stem cells to neuroblasts or astrocytes in saline (B) or METH (D) group, and GO or KEGG funtional enrichment of those genes. (E, F) Pseudotime expression graphs of 4 representative specific marker genes in these cell types showing the development tendency difference in saline (E) or METH (F) group.

6. The change of transcription factor regulatory network is also the cause of cognitive decline caused by METH.

We conducted an analysis of the differential expression of transcription factors in each cell type between METH and Saline mice (Fig.6.A and B). Subsequently, we constructed networks of transcription factor-target genes to predict changes in cellular functions (Fig.6.D-H, SI.3).

In astrocytes, a total of 42 differentially expressed transcription factors (DETFs) were identified (Fig.6.C), and their associated target genes were enriched in biological

717 processes related to neurogenesis and development, cognitive function, regulation of
718 inflammatory responses, as well as signaling pathways including PI3K-Akt, MAPK,
719 and cytokine-cytokine receptor interactions, among others (Fig.6.D).

720 Similarly, endothelial cells exhibited 48 DETFs, whose target genes were also
721 enriched in biological processes related to neural development, including
722 axonogenesis, neuronal differentiation, and functions associated with learning and
723 memory. Endothelial cells share common signaling pathways with astrocytes, such as
724 PI3K-Akt and MAPK (Fig.6.E). Furthermore, biological processes specifically
725 associated with endothelial cells, such as endothelial cell proliferation, cell-cell
726 adhesion, and cell junction assembly, were found to be involved in signaling pathways
727 including Ras, focal adhesion, and Wnt, among others.

728 Although only 29 DETFs were identified in microglia, they play a significant
729 regulatory role in processes such as membrane potential modulation, axonogenesis,
730 and neuronal death. These biological processes are closely associated with synaptic
731 pruning and neuronal survival, which may ultimately contribute to cognitive
732 dysfunction. Signaling pathways including calcium, Wnt, cGMP, and cAMP are
733 actively involved in the aforementioned processes (Fig.6.F).

734 As key supporters of neuronal bodies and axons, oligodendrocytes exhibit 32
735 DETFs that regulate processes related to cytoskeletal fiber organization and axon
736 development. This suggests that METH exposure disrupts the transcriptional
737 regulation of genes involved in neural support, thereby increasing neuronal
738 vulnerability to damage. These effects may be mediated through signaling pathways
739 such as Hippo, FoxO, Apelin, and Focal Adhesion. Whether the transcriptional
740 disruption affects neuronal growth itself or the maintenance of surrounding cells and
741 the neural environment under chronic METH treatment remains an important factor
742 contributing to cognitive decline in mice.

743 Interestingly, neurons derived from NSCs exhibit the highest and second-highest
744 numbers of DETFs, respectively, and share highly similar functional enrichment terms

among their target genes. These terms are primarily associated with neurodegenerative processes such as autophagy and neuronal death, axonogenesis, ameboid cell migration, and biosynthetic activities, which are also comparable to those observed in neuroblasts (Fig.6.H). This indicates that METH may exert common neurotoxic mechanisms in both mature neurons and neural precursor cells by modulating similar pathways through the expression of differentially regulated neural transcription factors.

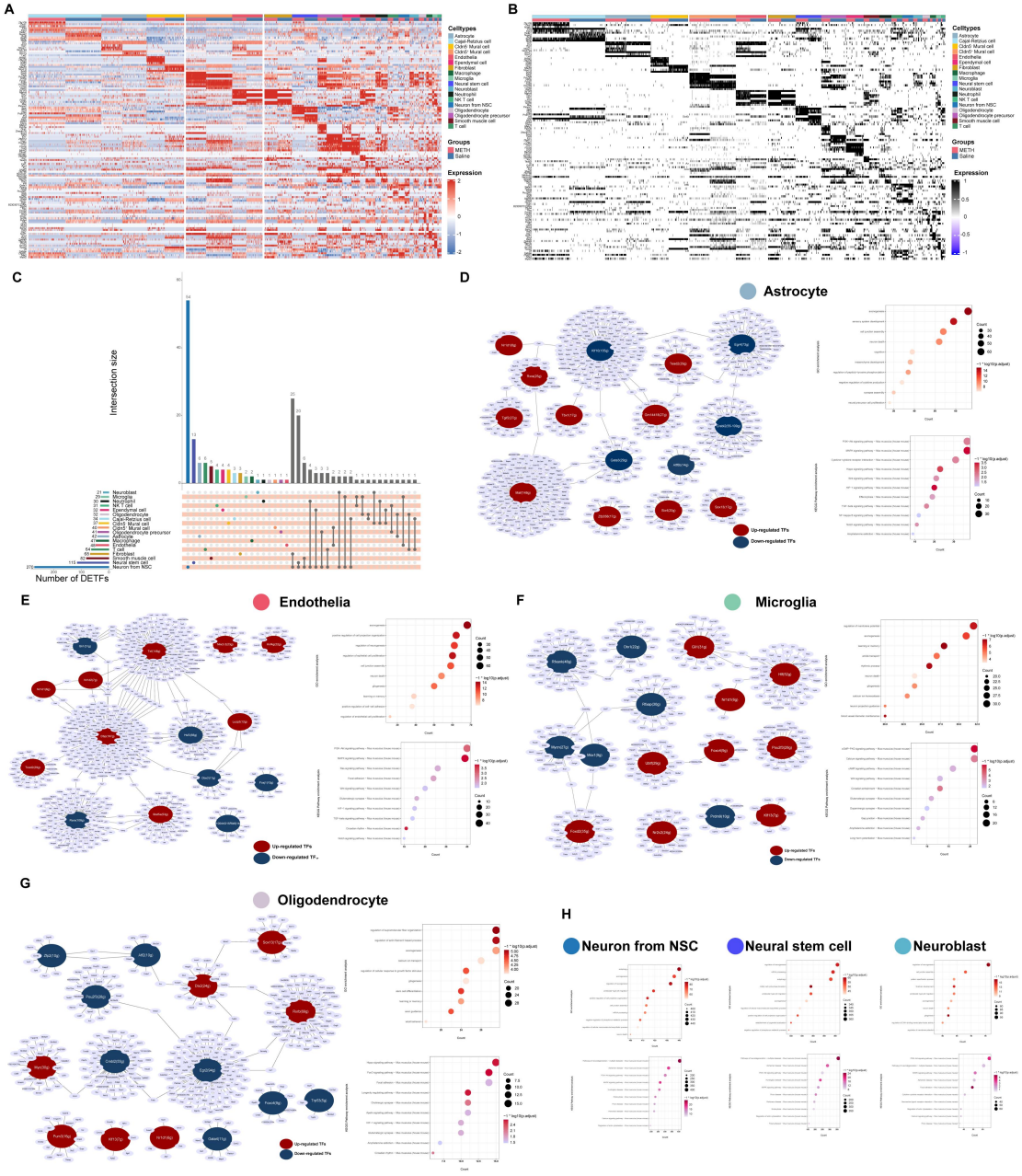

Fig.6. Transcription factor (TF) analysis and function prediction. (A-B) Heatmap of the average expression and the area under the curve scores of TF motifs estimated per cell by SCENIC. Shown are top five differentially activated motifs in each cell type of saline and METH groups, respectively. (C) The upset plot showing the number of all of unique and some of shared TFs of hippocampal cell types. (D-G) Gene regulatory network analysis and function enrichment using top 10 of SCENIC identifies critical TFs of astrocytes, endothelia, microglia and oligodendrocytes. (H) Enrichment analysis of target genes predicted by TFs of neuronal development related cell types (Neuron from NSC, NSC and neuroblast).

Discussion

As a psychostimulant drug widely use in worldwide, METH can elevate the risk to various neurological neuropsychiatric disorders due to its addictive and neurotoxic effect. In our study, animal behavior experiments illustrate that chronic METH abuse can cause cognitive decline in mice, which is manifested in spatial cognition, working memory and new object learning. Although previous studies also have similar concusions of METH-induced learning and memory impairments and put forward a variety of therapeutic improvement schemes (e.g. melatonin, oxytocin, housing and tetrahydropalmatine)(27-30), it seems that there are few practical, effective, and recognized treatments for chronic METH abuse-induced cognitive dysfunction therapy. Because researchers have found that METH can affect many organs throughout the body including most areas of the brain by complex and diverse molecular mechanisms, mainly involving excitatory toxicity, neurotransmitter disruption, oxidative stress, cytotoxicity (apoptosis, necrosis, and autophagy), inflammatory response, metabolism disorder et al(31-33). Furthermore, unlike acute METH-induced injury, chronic METH abuse represents a more complex process characterized by concurrent neurotoxic damage and reparative responses(34-36).

The hippocampus plays an essential role in a range of advanced brain functions, including memory and emotional regulation, and spatial navigation, and its impairment

780 or dysfunction have been proved to closely associate with neuropsychological
781 diseases like neurodegeneration, affective disturbance, and learning disabilities(37).

782 On the base of our animal behavior results, we used scRNA-seq to investigate all
783 mouse hippocampal cell types except for mature neurons and to explain the
784 heterogeneity of METH effects between different types of cells and provide more
785 targeted mechanisms for METH-induced neurotoxicity and targets for precise therapy.
786 Given that this study aims to capture the complete mRNA expression profile of intact
787 cells, we employed scRNA-seq technology. In contrast to single-cell nucleus
788 sequencing (snRNA-seq), this approach necessitates that cells be maintained under
789 conditions as close to physiological states as possible, thereby requiring high
790 structural integrity, robust viability, and minimal exposure to external perturbations.
791 Accordingly, during sample collection and the preparation of single-cell suspensions,
792 we processed the tissues as rapidly and gently as feasible. Nevertheless, mature
793 neurons — due to their highly differentiated state, limited deformability, and the
794 presence of long axons — are particularly susceptible to damage or functional
795 inactivation during the dissociation process, and are therefore frequently excluded
796 prior to sequencing. Therefore, we propose that the neurons captured in this study
797 predominantly represent immature neurons or a distinct subpopulation of neurons
798 with relatively smaller cell bodies. Although we did not detect the expression profiles
799 of mature neuronal genes, our dataset provides a comprehensive and detailed
800 characterization of various non-neuronal cell types. Each analyzed cell contains the
801 complete mRNA expression profile, which accurately reflects its functional state.
802 Accumulating evidence indicates that non-neuronal cell populations in the brain play a
803 critical role in chronic neurodegenerative diseases, with their functional states
804 significantly influencing neuronal activity and serving as potential early biomarkers,
805 contributors to disease pathogenesis, and therapeutic targets(38, 39). Notably, the
806 cognitive impairments induced by chronic METH exposure exhibit certain pathological
807 similarities to those observed in Alzheimer's disease and Parkinson's disease(40, 41).
808 Our dataset offers valuable insights into the functional alterations, predictive dynamics,

809 and intercellular communication of non-neuronal cells following chronic METH
810 exposure, thereby providing robust biological information to enhance our
811 understanding of METH-induced neurotoxicity and cognitive dysfunction.

812 1. Revealing a novel pattern of neuronal death and elucidating the impact of neuronal
813 interactions with other cells during development and maturation.

814 METH can cause abnormal neuronal function in various direct or indirect ways.
815 METH has a direct toxic effect on neurons causing neuronal damage by various
816 programmed cell death, such as apoptosis, autophagy, necroptosis, pyroptosis, and
817 ferroptosis(42). In spite of mature neurons loss during dissociation, we still isolated the
818 neurons remaining a few NSC markers in some degrees and we considered these
819 neurons developed from NSCs on account of that adult hippocampal neurogenesis is
820 a continuous process. Consistent with previous results, we found a few genes of
821 these neurons related to multiple neuron death biological processes exist
822 differences. For example, Cebpb mediate endoplasmic reticulum stress by
823 Nupr1-C/EBP homologous protein (CHOP) pathway, Prnp/Psenen/apoe are
824 associated with neurodegeneration disease in amyloid-beta metabolic process,
825 Gsk3b increases phosphorylation of Tau, Ddrgk1/Mcl1/Sh3glb1 play important role in
826 mitochondrial autophagy, ATF3 forms dimer with c-Jun to promote apoptosis(43). We
827 also noticed TNF superfamily cytokines and ILs overexpression in these neurons may
828 attracts microglia or actives astrocytes leading to neuron death. Abnormal neuronal
829 function is also indirectly related to METH's effects on various auxiliary cells. Our
830 cellchat data showed these neurons generating more communication signals to
831 vascular cells, fibroblasts and ependymal cells after chronice METH treatment. As
832 sources, these neurons upregulate signals like Vegf (Vascular endothelial growth
833 factor, promoting blood vessel growth and increasing permeability.), Sema3b and
834 Sema3c(are critical for neuron projection, guidance of axons, dendritic spine pruning
835 and ECs repulsion(44-46)), Ptn and Mdk (Pleiotrophin and Midkine, as neurotrophic
836 factors, is critical in different steps of differentiation of different cells both in
837 development and in wound repair, especially in neural regeneration, and is

838 up-regulated in drug abuser and neurodegenerative diseases patient(47).), Igf2
839 (Insulin-like growth factor 2, emerged as a critical molecule of synaptic plasticity and
840 learning and memory(48).), and Cxcl12 (concerning about regulating generation,
841 positioning and maturation of new neurons(49, 50), as well as the communication with
842 blood vessels(51).), but downregulate signals like Bmp6 (Bmp6 level shows an
843 increase in AD-related neurogenic deficits(52), and critical functions to EC
844 differentiation(53).), Bmp7 (Bmp7 expression in radial glial cells may promotes
845 neurogenesis, inhibits gliogenesis(54).), and Fgf2 (a crucial molecule modulating cell
846 proliferation and survival in central nervous system(55).). As receptors, there neurons
847 recept signals from vascular cells mainly about extracellular matrix, such as Col
848 (collagen) families and Lam (laminin) families. Our analysis showed METH impedes
849 the neuronal maturation process which closely relied on the regulation of vascular
850 cells (Fig.7).

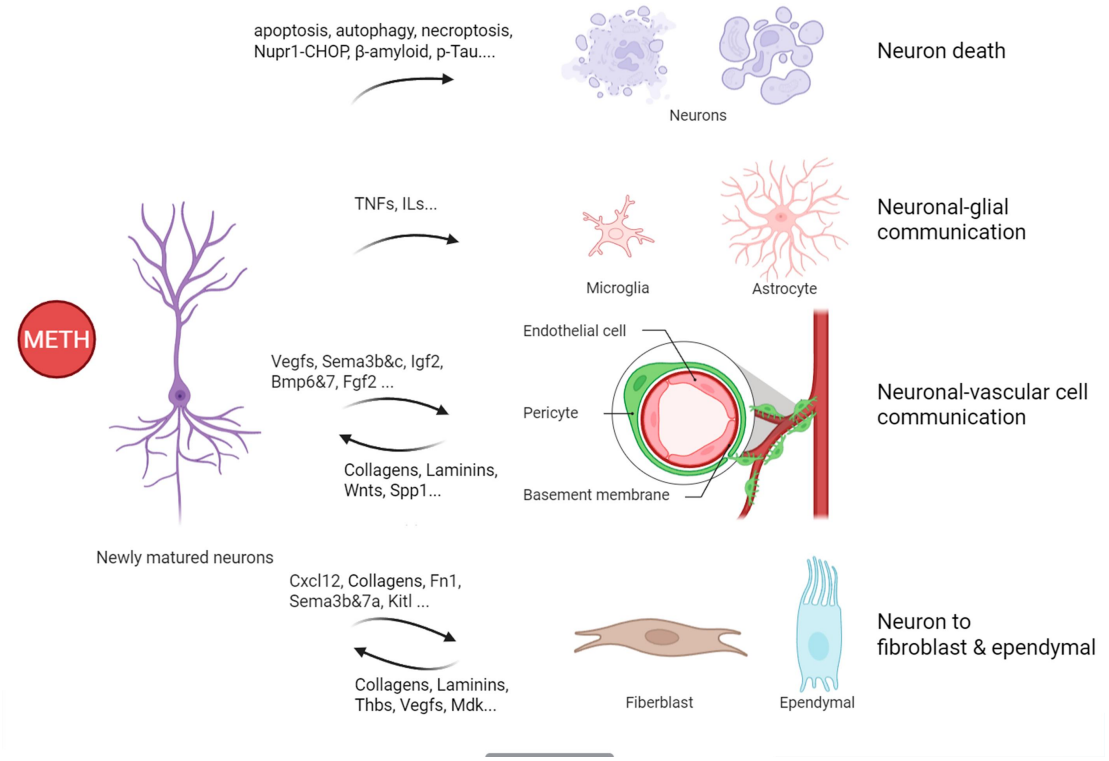

851

852 Fig.7. A schematic illustration of the effects of METH on neuronal cell death during development and
853 maturation and its interactions with glias, vascular cells, fiberblast and ependymal.

854 2. Analysis of dynamic changes in neurogenesis to track spatiotemporal shifts in cell
855 composition, signaling, and functional integration during nervous system development
856 and regeneration.

857 METH can cause damage to neurons through various mechanisms, while also
858 have impacts on neural stem/progenitor cells. However, these impacts seem to be
859 different between researches of actue or chronic abuse, intermittent or continuous
860 administration, addiction or withdrawal(56-59). In the researche of chronic METH
861 abuse, it has reported that METH mainly has negetive effects on stem/progenitor cells
862 resulting decreasement proliferative and neurogenesis capacity(56, 60), and even cell
863 death(61, 62). Here our analysis provided in vivo evidences of neurogenesis
864 alterations under chronice METH abuse. We confirmed METH's neurotoxicity to
865 NSCs and progenitor cells like neuroblasts and CRs, and ulteriorly we used
866 pseudotime to explore its influences on differentiation process and dynamics of neural
867 stem cells. The variations of characteristic genes on each branches of neural
868 development trajectory may reveal inflection points in the direction alterations of NSC
869 development under METH effect. It is also necessary to emphsize accurate
870 quantifications of various types of cells counting in the neurogenetic locus will be
871 helpful to lucubrate the toxicity of METH on neurogenesis (Fig.8).

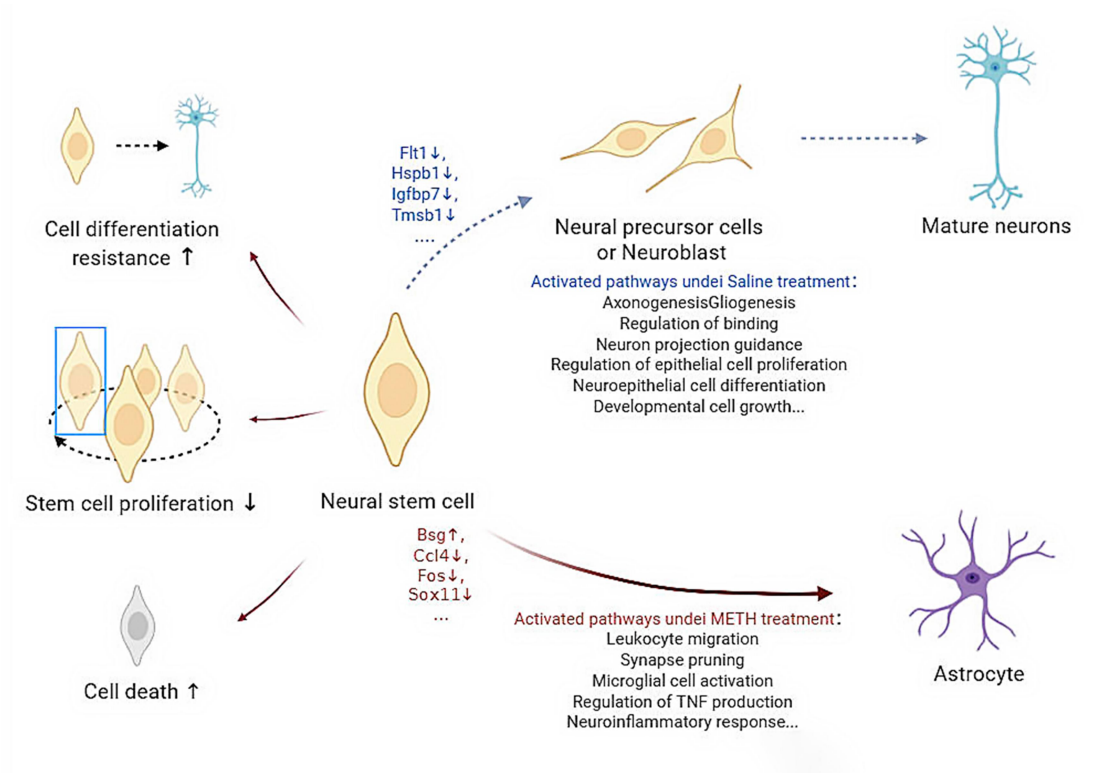

Fig.8. A schematic illustration of the effects of METH on cell proliferation capacity and cellular activity in neural stem cells, as well as associated alterations in gene expression and signaling pathways during their differentiation into neurons or astrocytes.

3. Establish a comprehensive cellular interaction map of the neurovascular unit

BBB injury is one of neurotoxic mechanisms of METH neurotoxicity, however, the impact of METH on BBB and its consequent effects on neural function far exceed the barrier dysfunction and abnormal substance transport mentioned in current researches. Previous studies of METH neurovascular toxicity have reported that ECs structure and function disorder and astrocytes-released cytokines or damage factors induced injury are parts of proper mechanisms for BBB injury(14), however these studies usually consider a single aspect of cell type or mechanism within BBB while current researches emphasize that neurovascular unit (NVU) comprises more informations about microcirculation integrity, vascular function and cellular cooperation, which are important to cognition regulation(63). In our study, we parsed most of NVU components which are consisted of ECs, mural cells, SMCs, gial cells

888 (astrocytes, oligodendrocytes and microglia), neurons and basal matrix. We found
889 that ECs can be grouped into several subsets may related to the difference between
890 arteries and veins and the grade of vascular branches, which make it possible to
891 anaylze endothelial dysfunctions like insufficient nutrient and oxygen transport, low
892 clearance efficiency of metabolic waste in cerebral circulation, or leukocyte adhesion
893 and migration. Moreover, mounting evidences correlate mechanical stress with
894 endothelial function, such as barrier function, inflammatory signaling, apoptosis,
895 oxidative stress, endothelial mesenchymal transformation and aging(64), which
896 means ECs located in different fluid states of vascular segments may be regulated
897 variously as results of METH-induced cerebral blood flow abnormalities(65-67). In the
898 meanwhile, the influence of the endothelium on other cell types is extensive, including
899 but not limited to vascular tone or structure, maintenance of collateral vessels,
900 neurotransmission and neurogenesis(63), as our DEGs analysis found that the effects
901 of METH on ECs are not only to damage the junction structure and cause autophagy
902 apoptosis, but also to change the association with other cells, such as GO terms:
903 vesicle-mediated transport in synapse, neurotransmitter transport, or glial cell
904 proliferation. Although there are few METH-induced neurovascular toxicity researches
905 concerning mural cells, who are thought to include pericytes, SMCs and
906 fibroblasts(68), we tried to distinguish them by expression levels of maker genes and
907 eliminate the effect of doublets, and we interestingly found that they share many
908 common genic features as ECs and SMCs, of which some of mural cells have similar
909 expression levels of marker genes as ECs especially. As a result, we classified mural
910 cells as *Cldn5*$^{+}$ and *Cldn5*$^{-}$ mural cells by the similarity to ECs, and we assumed that
911 the diversity of mural cell's functions depends on their proximity and interaction
912 degree to other vascular cells, which is reflecting cellular collaboration in NVU.

913 4. Chronic METH exposure triggers neuroinflammation through coordinated
914 interactions among immune cells in the central nervous system and peripheral
915 compartments.

Traditional METH research has always linked neuroinflammation to astrocytes, microglia, or certain neuroinflammatory factors, but in recent years, the functions of immune cells residing in neural tissue and the neural immune system deserve our attention. Different neural inflammatory factors or immune signals drive different cellular responses through various signaling pathways. As specialized immune cells of the central nervous system, microglia dominate neuroinflammatory processes under chronice METH exposure and play roles as initiators and executors. We found that microglia in our model up-regulates immune and inflammatory responses, such as MHC class II reaction, IL-1 / IL-2 / IL-6 / TNF superfamily cytokines production, and we also noticed that microglia strengthen communications with astrocytes, leukocytes, and lymphocytes whose bioprocesses include activation, differentiation, chemotaxis and migration. It has provided that TNF-α, IL-1α and C1q released by microglia can induce astrocytes to transform into neurotoxic phenotype cells(69). Recent researches pay more attention to the interaction of central and peripheral immune cells influencing neurodegenerations by various mechanisms. Xiaoying Chen et al. reported activate microglia encoding more MHC Ⅰ and Ⅱ proteins recruit T cells into brain parenchyma resulting encephalanalosis(70). Besides, by these innate immune factors, microglia can react to METH-induced DAMPs (Damage Associated Molecular Patterns) from neurons or other cells. We also noticed that some of characteristic cellchat signals induced by METH (such as TIGIT, RANKL, SN, SPP1) are mainly caused by these peripheral immune cells espcially NK-T cells. Astrocytes reshape their morphological, genomic, metabolic, and functional characteristics in response to acute or chronic pathological stimuli through a process called reactive astrogliosis(71). Althought we found astrocytes as a whole can regulate inflammatory response, their functions of different subgroups still need to be classfied by genomic and functional features related to their location and interactions with other cells in the CNS. Specially, we noticed second-messenger-mediated signaling-cAMP is up-regulated in astrocytes, and it may act as a molecular switch for neuroprotective astrocyte reactivity(72). A variety of cells and factors in hippucampal microenvironment participate in or influence neuroinflammation after METH exprosure, our data

broadened the research field of neuroinflammation and provided valuable reference genes for various potential inflammatory participants (Fig.9).

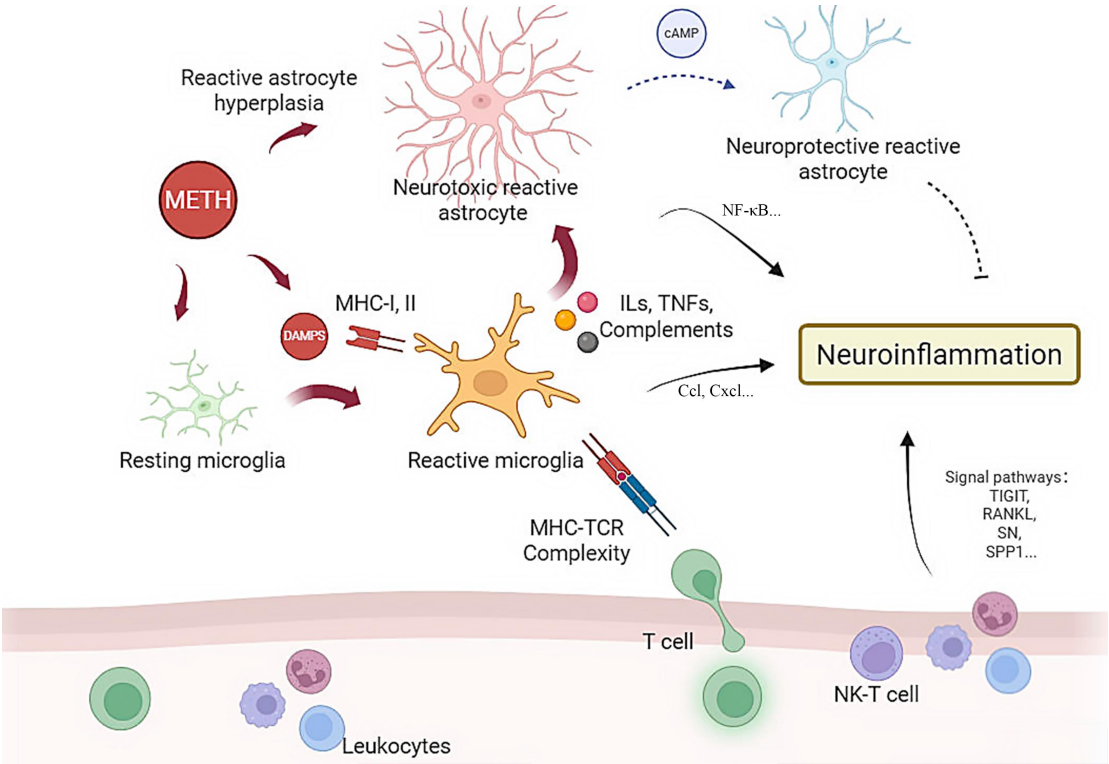

Fig.9. A schematic illustration of the mechanisms underlying neuroinflammation induced by chronic METH exposure. METH induces the reactive activation of microglia and astrocytes via multiple signaling pathways and facilitates the recruitment of peripheral lymphocytes and leukocytes to the central nervous system, thereby contributing to the complex regulatory mechanisms underlying the neuroinflammatory response.

5. Identification of disrupted metabolic and circadian coordination across diverse cell types.

The metabolism of various cells effected by METH in the hippocampus can not be ignored, as this may also be the cause or result of changes in cell functions. We have paid particular attention to changes in the metabolism of oligodendrocytes, as it is closely related to the support of neural function and structure.we have found that metabolic processes such as the production of organic acids, amino acids, glycerolipids, and glycolipids occur in oligodendrocytes and are similar to the changes

962 in the expression of lipid transport genes emphasized in AD, which may lead to
963 disruptions in myelin formation or energy supply to neurons(73). Furthermore,
964 endothelial cells and Cldn5^{+} enterocytes both showed impairments in lipid transport,
965 localization, and metabolism, involving genes such as *Slc2a1*, *Mfsd2a*, *Spp1*, *Apoe*,
966 the *Atp* family, and the *Abca* family. While current research suggests that the
967 characteristics of the BBB in a healthy state are not dependent on the maintenance of
968 microglial cells, the microglial scavenger PLX5622 has been found to impact
969 endothelial cholesterol metabolism(74). Additionally, impaired lipid metabolism in
970 microglial cells is considered an important pathogenic factor in AD(75). So we
971 hypothesize that endothelial and epithelial cell lipid metabolism and transport
972 disorders triggered by METH may promote lipid accumulation in microglia and cause
973 neurological damage.

974 The disruption of circadian rhythms has rarely been mentioned in previous
975 studies on METH, but METH, as a neurostimulant drug often used in nightlife, can
976 affect sleep. Interestingly, the frequent occurrence of circadian regulation in our
977 analysis of a number of cell-types is also worthy of attention, e.g. Genes involved in
978 circadian rhythm regulation, like *Per2*, *Per3, Ciart*, *Nr1d1* or *Nr1d2,* are up-regulated
979 in gliocytes such as astrocytes, oligodendrocytes and microglia, *Nrd1*, *Nrd2*, *Sfpq*
980 (regulates the circadian clock by repressing the transcriptional activator activity of the
981 CLOCK-ARNTL heterodimer(76)) are up-regulated in macrophage. Recent research
982 had reported that the circadian clock regulates the immune response of various
983 peripheral innate and adaptive immune cell types and astrocytes and microglia also
984 possess functioning circadian clocks, and circadian timing can affect their
985 inflammatory response, which may be the regulatory mechanism of
986 neuroinflammation in AD(77). Moreover, we noticed that circadian rhythm disorder in
987 endothelia (involving *Per2*, *Cry2*, *Cry1* and *Ptger4*) , smooth muscle cells (involving
988 *Cavin3*, *Kmt2a*, *Per1*, *Nr1d2* et al.) and ependymal cells (involving *Phlpp1*, *Ptgds*,
989 *Clock*, *Id2*). Existing researches showed that the clearance of metabolites, transporter
990 function, permeability, vascular inflammatory and vasomotion of BBB are regulated by

991 circadian rhythm(78-80). A few studies of METH abuse were concerned about
992 circadian rhythm disorder and reported that METH-associated heart failure(81),
993 variability of body temperature(82), Learned motivation(83), addictive properties(84)
994 and learning and memory impairments(28) are affected by disrupted circadian rhythms.
995 However it still needs more researches to figure out the mechanisms of circadian
996 rhythm disturbed by METH and how does circadian rhythm disruption cause METH
997 toxicity.

998 Conclusion

999 In conclusion, our reaserch provides scRNA data on the changes of various types
1000 of cells in the hippocampus of mice with cognitive impairment caused by METH
1001 exposure. These results provide new insights while partially confirming the results of
1002 previous studies on METH neurotoxicity. And we will conduct more confirmatory work
1003 in the future to elucidate the mechanisms of neurotoxicity and cognitive decline
1004 caused by chronic METH abuse.

1005 Ethics approval and consent to participate

1006 All protocols approved by the Institutional Animal Care and Use Committee in
1007 Southern Medical University (Ethical number: L2022125), and consistent with NIH
1008 Guidelines for the Care and Use of Laboratory Animals (8th Edition, U.S. National
1009 Research Council, 2011).

1010 Consent for publication

1011 All authors have approved the manuscript and this submission.

1012 Funding

1013 This work was supported by the Research Projects of National Natural Science
1014 Foundation of China (No.82271930) and GuangDong Basic and Applied Basic
1015 Research Foundation (2024A1515013050, 2021A1515010909 and
1016 2022A1515110743). The research platforms were supported by Southern Medical

University (SMU), Institute of forensic medicine of SMU. We thank Seekgene Biotechnology Co., Ltd for helpful technical support.

Authors and Affiliations

School of Forensic Medicine, Southern Medical University, Guangzhou 510515, Guangdong province, People' s Republicof China: DF Qiao, H Qiu, X Yue, YB Huang, ZL Meng.

Cancer Research Institute, School of Basic Medical Sciences, Southern Medical University, Guangzhou 510515, China: JH Wang.

Corresponding author: Correspondence to JH Wang and DF Qiao.

Authors' contributions

H Qiu: Conceptualization, Experiments, Data Collection, Statistical Analysis, Sing cell Data Analysis, Writing (Original Draft), Writing (Editing). X Yue, YB Huang and ZL Meng: Animal treatments and Behavior data analysis. JH Wang: Sing-cell Data Analysis, Funding. DF Qiao: Supervision, Funding, Writing (Editing).

Conflict of Interest

The authors declare that they have no known competing financial interests or personal relationships that could have appeared to influence the work reported in this paper.

Availability of data and material

The single-cell RNA-seq data that support findings of this study are available in Gene Expression Omnibus (GEO) under accession numbers GSE252939. Other experimental data and data analysis code can be obtained from the corresponding author at request.

Reference

1. UNODC TUNO.,World Drug Report 2023 (United Nations publication, 2023). www.unodc.org/unodc/en/data-and-analysis/world-drug-report-2023.html., 2023.

2. Thompson PM, Hayashi KM, Simon SL, Geaga JA, Hong MS, Sui Y *et al.*. Structural abnormalities in the brains of human subjects who use methamphetamine. *J NEUROSCI* 2004 2004/6/30; **24**(26)**:** 6028-6036.

3. MacDuffie KE, Brown GG, McKenna BS, Liu TT, Meloy MJ, Tawa B *et al.*. Effects of HIV Infection, methamphetamine dependence and age on cortical thickness, area and volume. *NEUROIMAGE-CLIN* 2018 2018/1/20; **20:** 1044-1052.

4. Schwartz DL, Mitchell AD, Lahna DL, Luber HS, Huckans MS, Mitchell SH *et al.*. Global and local morphometric differences in recently abstinent methamphetamine-dependent individuals. *NEUROIMAGE* 2010 2010/5/1; **50**(4)**:** 1392-1401.

5. Dean AC, Groman SM, Morales AM, London ED. An evaluation of the evidence that methamphetamine abuse causes cognitive decline in humans. *NEUROPSYCHOPHARMACOL* 2013 2013/1/1; **38**(2)**:** 259-274.

6. Guerin AA, Bridson T, Plapp HM, Bedi G. A systematic review and meta-analysis of health, functional, and cognitive outcomes in young people who use methamphetamine. *NEUROSCI BIOBEHAV R* 2023 2023/10/1; **153:** 105380.

7. Marshall JF, Belcher AM, Feinstein EM, O'Dell SJ. Methamphetamine-induced neural and cognitive changes in rodents. *ADDICTION* 2007 2007/4/1; **102 Suppl 1:** 61-69.

8. Shukla M, Vincent B. Methamphetamine abuse disturbs the dopaminergic system to impair hippocampal-based learning and memory: An overview of animal and human investigations. *NEUROSCI BIOBEHAV R* 2021 2021/12/1; **131:** 541-559.

9. Jin S, Guerrero-Juarez CF, Zhang L, Chang I, Ramos R, Kuan CH *et al.*. Inference and analysis of cell-cell communication using CellChat. *NAT COMMUN* 2021 2021/2/17; **12**(1)**:** 1088.

10. Qiu X, Mao Q, Tang Y, Wang L, Chawla R, Pliner HA *et al.*. Reversed graph embedding resolves complex single-cell trajectories. *NAT METHODS* 2017 2017/10/1; **14**(10)**:** 979-982.

11. Van de Sande B, Flerin C, Davie K, De Waegeneer M, Hulselmans G, Aibar S *et al.*. A scalable SCENIC workflow for single-cell gene regulatory network analysis. *NAT PROTOC* 2020 2020/7/1; **15**(7)**:** 2247-2276.

12. Herrmann C, Van de Sande B, Potier D, Aerts S. i-cisTarget: an integrative genomics method for the prediction of regulatory features and cis-regulatory modules. *NUCLEIC ACIDS RES* 2012 2012/8/1; **40**(15)**:** e114.

13. Sweeney MD, Zhao Z, Montagne A, Nelson AR, Zlokovic BV. Blood-Brain Barrier: From Physiology to Disease and Back. *PHYSIOL REV* 2019 2019/1/1; **99**(1)**:** 21-78.

14. Pang L, Wang Y. Overview of blood-brain barrier dysfunction in methamphetamine abuse. *BIOMED PHARMACOTHER* 2023 2023/5/1; **161:** 114478.

15. Obermeier B, Daneman R, Ransohoff RM. Development, maintenance and disruption of the blood-brain barrier. *NAT MED* 2013 2013/12/1; **19**(12)**:** 1584-1596.

16. Li S, Sheng ZH. Oligodendrocyte-derived transcellular signaling regulates axonal energy metabolism. *CURR OPIN NEUROBIOL* 2023 2023/6/1; **80:** 102722.

17. Lezmy J, Arancibia-Carcamo IL, Quintela-Lopez T, Sherman DL, Brophy PJ, Attwell D. Astrocyte Ca(2+)-evoked ATP release regulates myelinated axon excitability and conduction speed. *SCIENCE* 2021 2021/10/15; **374**(6565)**:** eabh2858.

18. Geigenmuller JN, Tari AR, Wisloff U, Walker TL. The relationship between adult hippocampal neurogenesis and cognitive impairment in Alzheimer's disease. *ALZHEIMERS DEMENT* 2024 2024/10/1; **20**(10)**:** 7369-7383.

19. Gengatharan A, Malvaut S, Marymonchyk A, Ghareghani M, Snapyan M, Fischer-Sternjak J *et al.*. Adult neural stem cell activation in mice is regulated by the day/night cycle and intracellular calcium dynamics. *CELL* 2021 2021/2/4; **184**(3)**:** 709-722.

20. Riva M, Moriceau S, Morabito A, Dossi E, Sanchez-Bellot C, Azzam P *et al.*. Aberrant survival of hippocampal Cajal-Retzius cells leads to memory deficits, gamma rhythmopathies and susceptibility to seizures in adult mice. *NAT COMMUN* 2023 2023/3/18; **14**(1)**:** 1531.

21. Anstotz M, Lee SK, Maccaferri G. Glutamate released by Cajal-Retzius cells impacts specific hippocampal circuits and behaviors. *CELL REP* 2022 2022/5/17; **39**(7)**:** 110822.

22. Rogers K. "ependymal cell".Encyclopedia Britannica, 5 Dec. 2018.

1119
1120 23. Plikus MV, Wang X, Sinha S, Forte E, Thompson SM, Herzog EL *et al.*. Fibroblasts: Origins,
1121 definitions, and functions in health and disease. *CELL* 2021 2021/7/22; **184**(15)**:** 3852-3872.
1122
1123 24. Yeini E, Ofek P, Pozzi S, Albeck N, Ben-Shushan D, Tiram G *et al.*. P-selectin axis plays a key
1124 role in microglia immunophenotype and glioblastoma progression. *NAT COMMUN* 2021 2021/3/26;
1125 **12**(1)**:** 1912.
1126
1127 25. Cardone J, Le Friec G, Kemper C. CD46 in innate and adaptive immunity: an update. *CLIN EXP*
1128 *IMMUNOL* 2011 2011/6/1; **164**(3)**:** 301-311.
1129
1130 26. Cope EC, Gould E. Adult Neurogenesis, Glia, and the Extracellular Matrix. *CELL STEM CELL*
1131 2019 2019/5/2; **24**(5)**:** 690-705.
1132
1133 27. Chen YJ, Liu YL, Zhong Q, Yu YF, Su HL, Toque HA *et al.*. Tetrahydropalmatine protects against
1134 methamphetamine-induced spatial learning and memory impairment in mice. *NEUROSCI BULL*
1135 2012 2012/6/1; **28**(3)**:** 222-232.
1136
1137 28. Veschsanit N, Yang JL, Ngampramuan S, Viwatpinyo K, Pinyomahakul J, Lwin T *et al.*.
1138 Melatonin reverts methamphetamine-induced learning and memory impairments and hippocampal
1139 alterations in mice. *LIFE SCI* 2021 2021/1/15; **265:** 118844.
1140
1141 29. Fan XY, Yang JY, Dong YX, Hou Y, Liu S, Wu CF. Oxytocin inhibits
1142 methamphetamine-associated learning and memory alterations by regulating DNA methylation at the
1143 Synaptophysin promoter. *ADDICT BIOL* 2020 2020/1/1; **25**(1)**:** e12697.
1144
1145 30. Gutierrez A, Jablonski SA, Amos-Kroohs RM, Barnes AC, Williams MT, Vorhees CV. Effects of
1146 Housing on Methamphetamine-Induced Neurotoxicity and Spatial Learning and Memory. *ACS*
1147 *CHEM NEUROSCI* 2017 2017/7/19; **8**(7)**:** 1479-1489.
1148
1149 31. Jayanthi S, Daiwile AP, Cadet JL. Neurotoxicity of methamphetamine: Main effects and
1150 mechanisms. *EXP NEUROL* 2021 2021/10/1; **344:** 113795.
1151
1152 32. Limanaqi F, Busceti CL, Celli R, Biagioni F, Fornai F. Autophagy as a gateway for the effects of
1153 methamphetamine: From neurotransmitter release and synaptic plasticity to psychiatric and
1154 neurodegenerative disorders. *PROG NEUROBIOL* 2021 2021/9/1; **204:** 102112.
1155
1156 33. Shrestha P, Katila N, Lee S, Seo JH, Jeong JH, Yook S. Methamphetamine induced neurotoxic
1157 diseases, molecular mechanism, and current treatment strategies. *BIOMED PHARMACOTHER* 2022
1158 2022/10/1; **154:** 113591.
1159
1160 34. Bowyer JF, Sarkar S, Tranter KM, Hanig JP, Miller DB, O'Callaghan JP. Vascular-directed
1161 responses of microglia produced by methamphetamine exposure: indirect evidence that microglia are
1162 involved in vascular repair? *J NEUROINFLAMM* 2016 2016/3/12; **13**(1)**:** 64.

35. Ghosh M, Pearse DD. The Yin and Yang of Microglia-Derived Extracellular Vesicles in CNS Injury and Diseases. *CELLS-BASEL* 2024 2024/11/6; **13**(22).

36. Chiareli RA, Carvalho GA, Marques BL, Mota LS, Oliveira-Lima OC, Gomes RM *et al.*. The Role of Astrocytes in the Neurorepair Process. *FRONT CELL DEV BIOL* 2021 2021/1/20; **9:** 665795.

37. Lazarov O, Hollands C. Hippocampal neurogenesis: Learning to remember. *PROG NEUROBIOL* 2016 2016/3/1; **138-140:** 1-18.

38. Castellani G, Croese T, Peralta RJ, Schwartz M. Transforming the understanding of brain immunity. *SCIENCE* 2023 2023/4/7; **380**(6640)**:** eabo7649.

39. Uddin MS, Lim LW. Glial cells in Alzheimer's disease: From neuropathological changes to therapeutic implications. *AGEING RES REV* 2022 2022/6/1; **78:** 101622.

40. Lappin JM. Rare but relevant: Methamphetamine and Parkinson's disease. *ADDICTION* 2025 2025/4/1; **120**(4)**:** 797-800.

41. Shukla M, Vincent B. The multi-faceted impact of methamphetamine on Alzheimer's disease: From a triggering role to a possible therapeutic use. *AGEING RES REV* 2020 2020/7/1; **60:** 101062.

42. Guo D, Huang X, Xiong T, Wang X, Zhang J, Wang Y *et al.*. Molecular mechanisms of programmed cell death in methamphetamine-induced neuronal damage. *FRONT PHARMACOL* 2022 2022/1/20; **13:** 980340.

43. Mei Y, Yuan Z, Song B, Li D, Ma C, Hu C *et al.*. Activating transcription factor 3 up-regulated by c-Jun NH(2)-terminal kinase/c-Jun contributes to apoptosis induced by potassium deprivation in cerebellar granule neurons. *NEUROSCIENCE* 2008 2008/2/6; **151**(3)**:** 771-779.

44. Falk J, Bechara A, Fiore R, Nawabi H, Zhou H, Hoyo-Becerra C *et al.*. Dual functional activity of semaphorin 3B is required for positioning the anterior commissure. *NEURON* 2005 2005/10/6; **48**(1)**:** 63-75.

45. Mohan V, Wade SD, Sullivan CS, Kasten MR, Sweetman C, Stewart R *et al.*. Close Homolog of L1 Regulates Dendritic Spine Density in the Mouse Cerebral Cortex Through Semaphorin 3B. *J NEUROSCI* 2019 2019/8/7; **39**(32)**:** 6233-6250.

46. Martins LF, Brambilla I, Motta A, de Pretis S, Bhat GP, Badaloni A *et al.*. Motor neurons use push-pull signals to direct vascular remodeling critical for their connectivity. *NEURON* 2022 2022/12/21; **110**(24)**:** 4090-4107.

47. Herradon G, Perez-Garcia C. Targeting midkine and pleiotrophin signalling pathways in addiction and neurodegenerative disorders: recent progress and perspectives. *BRIT J PHARMACOL* 2014

2014/2/1; **171**(4)**:** 837-848.

48. Alberini CM. IGF2 in memory, neurodevelopmental disorders, and neurodegenerative diseases. *TRENDS NEUROSCI* 2023 2023/6/1; **46**(6)**:** 488-502.

49. Trousse F, Jemli A, Silhol M, Garrido E, Crouzier L, Naert G *et al.*. Knockdown of the CXCL12/CXCR7 chemokine pathway results in learning deficits and neural progenitor maturation impairment in mice. *BRAIN BEHAV IMMUN* 2019 2019/8/1; **80:** 697-710.

50. Abe P, Wust HM, Arnold SJ, van de Pavert SA, Stumm R. CXCL12-mediated feedback from granule neurons regulates generation and positioning of new neurons in the dentate gyrus. *GLIA* 2018 2018/8/1; **66**(8)**:** 1566-1576.

51. Li M, Hale JS, Rich JN, Ransohoff RM, Lathia JD. Chemokine CXCL12 in neurodegenerative diseases: an SOS signal for stem cell-based repair. *TRENDS NEUROSCI* 2012 2012/10/1; **35**(10)**:** 619-628.

52. Crews L, Adame A, Patrick C, Delaney A, Pham E, Rockenstein E *et al.*. Increased BMP6 levels in the brains of Alzheimer's disease patients and APP transgenic mice are accompanied by impaired neurogenesis. *J NEUROSCI* 2010 2010/9/15; **30**(37)**:** 12252-12262.

53. Wu X, Yao J, Wang L, Zhang D, Zhang L, Reynolds EX *et al.*. Crosstalk between BMP and Notch Induces Sox2 in Cerebral Endothelial Cells. *CELLS-BASEL* 2019 2019/6/6; **8**(6).

54. Li Z, Liu G, Yang L, Sun M, Zhang Z, Xu Z *et al.*. BMP7 expression in mammalian cortical radial glial cells increases the length of the neurogenic period. *PROTEIN CELL* 2024 2024/1/3; **15**(1)**:** 21-35.

55. Tang MM, Lin WJ, Zhang JT, Zhao YW, Li YC. Exogenous FGF2 reverses depressive-like behaviors and restores the suppressed FGF2-ERK1/2 signaling and the impaired hippocampal neurogenesis induced by neuroinflammation. *BRAIN BEHAV IMMUN* 2017 2017/11/1; **66:** 322-331.

56. Mandyam CD, Wee S, Crawford EF, Eisch AJ, Richardson HN, Koob GF. Varied access to intravenous methamphetamine self-administration differentially alters adult hippocampal neurogenesis. *BIOL PSYCHIAT* 2008 2008/12/1; **64**(11)**:** 958-965.

57. Recinto P, Samant AR, Chavez G, Kim A, Yuan CJ, Soleiman M *et al.*. Levels of neural progenitors in the hippocampus predict memory impairment and relapse to drug seeking as a function of excessive methamphetamine self-administration. *NEUROPSYCHOPHARMACOL* 2012 2012/4/1; **37**(5)**:** 1275-1287.

58. Galinato MH, Lockner JW, Fannon-Pavlich MJ, Sobieraj JC, Staples MC, Somkuwar SS *et al.*. A synthetic small-molecule Isoxazole-9 protects against methamphetamine relapse. *MOL PSYCHIATR* 2018 2018/3/1; **23**(3)**:** 629-638.

1251
1252 59. Che X, Bai Y, Cai J, Liu Y, Li Y, Yin M *et al.*. Hippocampal neurogenesis interferes with
1253 extinction and reinstatement of methamphetamine-associated reward memory in mice.
1254 *NEUROPHARMACOLOGY* 2021 2021/9/15; **196:** 108717.
1255
1256 60. Wang S, Wang L, Bu Q, Wei Q, Jiang L, Dai Y *et al.*. Methamphetamine exposure drives cell
1257 cycle exit and aberrant differentiation in rat hippocampal-derived neurospheres. *FRONT*
1258 *PHARMACOL* 2023 2023/1/20; **14:** 1242109.
1259
1260 61. Baptista S, Bento AR, Goncalves J, Bernardino L, Summavielle T, Lobo A *et al.*. Neuropeptide Y
1261 promotes neurogenesis and protection against methamphetamine-induced toxicity in mouse dentate
1262 gyrus-derived neurosphere cultures. *NEUROPHARMACOLOGY* 2012 2012/6/1; **62**(7)**:** 2413-2423.
1263
1264 62. Bento AR, Baptista S, Malva JO, Silva AP, Agasse F. Methamphetamine exerts toxic effects on
1265 subventricular zone stem/progenitor cells and inhibits neuronal differentiation. *REJUV RES* 2011
1266 2011/4/1; **14**(2)**:** 205-214.
1267
1268 63. Yang Q, Wei X, Deng B, Chang Z, Jin D, Huang Y *et al.*. Cerebral small vessel disease alters
1269 neurovascular unit regulation of microcirculation integrity involved in vascular cognitive impairment.
1270 *NEUROBIOL DIS* 2022 2022/8/1; **170:** 105750.
1271
1272 64. McQueen A, Warboys CM. Mechanosignalling pathways that regulate endothelial barrier function.
1273 *CURR OPIN CELL BIOL* 2023 2023/10/1; **84:** 102213.
1274
1275 65. Li Y, Cui Z, Liao Q, Dong H, Zhang J, Shen W *et al.*. Support vector machine-based multivariate
1276 pattern classification of methamphetamine dependence using arterial spin labeling. *ADDICT BIOL*
1277 2019 2019/11/1; **24**(6)**:** 1254-1262.
1278
1279 66. Lafuente JV, Sharma A, Muresanu DF, Ozkizilcik A, Tian ZR, Patnaik R *et al.*. Repeated Forced
1280 Swim Exacerbates Methamphetamine-Induced Neurotoxicity: Neuroprotective Effects of Nanowired
1281 Delivery of 5-HT3-Receptor Antagonist Ondansetron. *MOL NEUROBIOL* 2018 2018/1/1; **55**(1)**:**
1282 322-334.
1283
1284 67. Ances BM, Vaida F, Cherner M, Yeh MJ, Liang CL, Gardner C *et al.*. HIV and chronic
1285 methamphetamine dependence affect cerebral blood flow. *J NEUROIMMUNE PHARM* 2011 2011/9/1;
1286 **6**(3)**:** 409-419.
1287
1288 68. Garcia FJ, Sun N, Lee H, Godlewski B, Mathys H, Galani K *et al.*. Single-cell dissection of the
1289 human brain vasculature. *NATURE* 2022 2022/3/1; **603**(7903)**:** 893-899.
1290
1291 69. Liddelow SA, Guttenplan KA, Clarke LE, Bennett FC, Bohlen CJ, Schirmer L *et al.*. Neurotoxic
1292 reactive astrocytes are induced by activated microglia. *NATURE* 2017 2017/1/26; **541**(7638)**:** 481-487.
1293
1294 70. Chen X, Firulyova M, Manis M, Herz J, Smirnov I, Aladyeva E *et al.*. Microglia-mediated T cell

infiltration drives neurodegeneration in tauopathy. *NATURE* 2023 2023/3/1; **615**(7953)**:** 668-677.

71. Lee HG, Lee JH, Flausino LE, Quintana FJ. Neuroinflammation: An astrocyte perspective. *SCI TRANSL MED* 2023 2023/11/8; **15**(721)**:** eadi7828.

72. Cameron EG, Nahmou M, Toth AB, Heo L, Tanasa B, Dalal R *et al.*. A molecular switch for neuroprotective astrocyte reactivity. *NATURE* 2024 2024/2/1; **626**(7999)**:** 574-582.

73. Murdock MH, Tsai LH. Insights into Alzheimer's disease from single-cell genomic approaches. *NAT NEUROSCI* 2023 2023/2/1; **26**(2)**:** 181-195.

74. Profaci CP, Harvey SS, Bajc K, Zhang TZ, Jeffrey DA, Zhang AZ *et al.*. Microglia are not necessary for maintenance of blood-brain barrier properties in health, but PLX5622 alters brain endothelial cholesterol metabolism. *NEURON* 2024 2024/9/4; **112**(17)**:** 2910-2921.

75. Haney MS, Palovics R, Munson CN, Long C, Johansson PK, Yip O *et al.*. APOE4/4 is linked to damaging lipid droplets in Alzheimer's disease microglia. *NATURE* 2024 2024/4/1; **628**(8006)**:** 154-161.

76. Balliu B, Durrant M, Goede O, Abell N, Li X, Liu B *et al.*. Genetic regulation of gene expression and splicing during a 10-year period of human aging. *GENOME BIOL* 2019 2019/11/4; **20**(1)**:** 230.

77. Lananna BV, McKee CA, King MW, Del-Aguila JL, Dimitry JM, Farias F *et al.*. Chi3l1/YKL-40 is controlled by the astrocyte circadian clock and regulates neuroinflammation and Alzheimer's disease pathogenesis. *SCI TRANSL MED* 2020 2020/12/16; **12**(574).

78. He J, Hsuchou H, He Y, Kastin AJ, Wang Y, Pan W. Sleep restriction impairs blood-brain barrier function. *J NEUROSCI* 2014 2014/10/29; **34**(44)**:** 14697-14706.

79. Cuddapah VA, Zhang SL, Sehgal A. Regulation of the Blood-Brain Barrier by Circadian Rhythms and Sleep. *TRENDS NEUROSCI* 2019 2019/7/1; **42**(7)**:** 500-510.

80. Zhang SL, Lahens NF, Yue Z, Arnold DM, Pakstis PP, Schwarz JE *et al.*. A circadian clock regulates efflux by the blood-brain barrier in mice and human cells. *NAT COMMUN* 2021 2021/1/27; **12**(1)**:** 617.

81. Zhang C, Chen C, Zhao X, Lu J, Zhang M, Qiu H *et al.*. New insight into methamphetamine-associated heart failure revealed by transcriptomic analyses: Circadian rhythm disorder. *TOXICOL APPL PHARM* 2022 2022/9/15; **451:** 116172.

82. Behrouzvaziri A, Zaretskaia MV, Rusyniak DE, Zaretsky DV, Molkov YI. Circadian variability of body temperature responses to methamphetamine. *AM J PHYSIOL-REG I* 2018 2018/1/1; **314**(1)**:** R43-R48.

83. Rawashdeh O, Clough SJ, Hudson RL, Dubocovich ML. Learned motivation drives circadian physiology in the absence of the master circadian clock. *FASEB J* 2017 2017/1/1; **31**(1)**:** 388-399.

84. Sayson LV, Lee HJ, Ortiz DM, Kim M, Custodio R, Lee CH *et al.*. The differential vulnerabilities of Per2 knockout mice to the addictive properties of methamphetamine and cocaine. *PROG NEURO-PSYCHOPH* 2023 2023/8/30; **126:** 110782.